Chapter 9
Friction Stir Processing

The intrinsic nature of friction stir process has two basic components as highlighted in previous chapters, material flow and microstructural evolution. The development of friction stir processing as a generic metallurgical tool for microstructural modification and a broader manufacturing technology is connected to these. Even though the adaption of these friction stir process based technological variants is slow, the potential of these is limitless. The focus of this chapter is to illustrate the linkages of basic friction stir process attributes to some illustrative examples of new technology development. The chapter is by no means comprehensive because many ideas can be built on these basics and each one can have its own niche area of application.

We start off with an overview Fig. 9.1 from Mishra and Mahoney (2007) that serves as a basic illustration. The material flow can be treated as the overarching aspect of all friction stir attributes other than temperature, but the split attributes listed are to facilitate visualization of microstructural evolution and development of the derivative processes, referred to as friction stir technologies. We have listed only (a) microstructural refinement, (b) homogenization and (c) primary particle breakdown, but other keywords can be used to describe the impact of friction stir process on key 'enabling' microstructural aspect for a particular friction stir technology. Let us take the first paper (Mishra et al. 1999) using the keyword 'friction stir processing' and related patent (Mishra and Mahoney 2004). As discussed in a bit more detail in the next section, fine grain size is a key enabling microstructural feature for superplasticity, as fine grain size is a necessary requirement for structural superplasticity. So, the sections below are setup with what are the key enabling microstructural aspect(s) and/or friction stir attribute(s) that leads to the development of a particular friction stir technology. The intention is that readers will not only find these examples illustrative, but also a foundational material that they can then use to develop additional friction stir technologies to broaden this generic processing tool. Significant part of the text presented below is based on an earlier review of Mishra and Mahoney (2007).

Another way to look at the opportunities of using friction stir processing is to consider a very well accepted set of design approaches and the materials science

R.S. Mishra et al., *Friction Stir Welding and Processing: Science and Engineering*,
DOI 10.1007/978-3-319-07043-8_9,

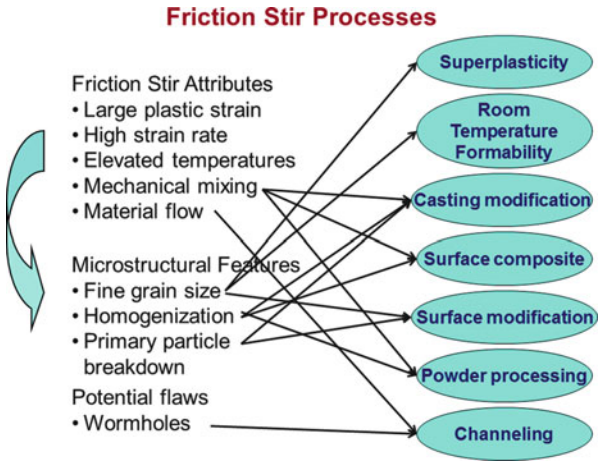

Fig. 9.1 An illustration of the evolution of microstructural features because of the basic friction stir process attributes, and its linkage to various emerging friction stir processing technologies (Mishra and Mahoney 2007, reprinted with permission from ASM International)

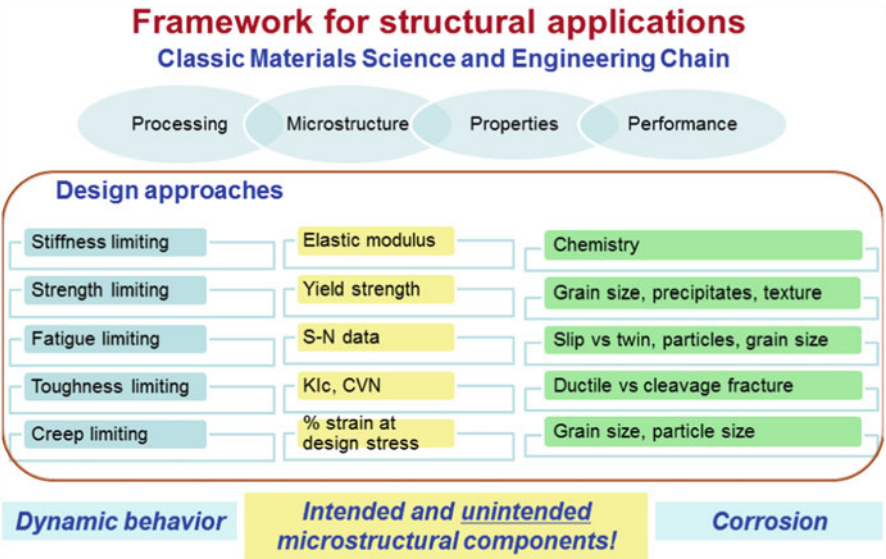

Fig. 9.2 A layout depicting the materials science and engineering chain along with five commonly used design approaches. The design approaches are linked with key materials properties and what they depend on

and engineering chain. Figure 9.2 shows this broad framework including dynamic and corrosion properties. A new keyword that is included is 'unintended microstructure'. A way to understand this is to think of how materials are used for engineering applications. The designer sets the performance goal and specifies

material that would meet the requirement. When a material is ordered, composition and minimum guaranteed properties are specified. A process may also be specified as a part of the design specification. What microstructure would give the properties is not a concern of the designer. The material composition combined with some typical manufacturing processing steps lead to 'intended' microstructure. A common observation is that impurity elements lead to unintended constitutive particles. One way to limit that is to specify tighter compositional control which has implication on price. Number of engineering failures are a result of these unintended microstructure or microstructural flaws. Friction stir processing can be used to modify these microstructural features, particularly the regions where finite element modeling tools show higher vulnerability.

9.1 Friction Stir Processing for Superplastic Forming

Superplasticity is an ability of a material to exhibit >200 % elongation in tension. Historically, a key aspect of the superplastic materials is also the low flow stress. In fact, the original development of superplastic forming in 1960s by Backofen et al. (1964) attracted more attention because it was gas forming of a metallic component. This gives an impression of ease of forming because one can conceptually visualize this as equivalent to glass blowing. Of course, once the formed metallic component cools down to room temperature, its properties are that of any structural metallic material. Superplastic forming grew rapidly in 1970s and 1980s, because of its ability to create 'unitized' components. Unitized components lower the number of parts that is used for a system. Aerospace industries were among the first adopters in spite of a major drawback of slow forming rate (strain rate of 10^{-4}–10^{-3} s^{-1}). Last 20 years or so there has been a large increase in efforts related to high strain rate superplasticity (strain rate $>10^{-2}$ s^{-1}).

9.1.1 Constitutive Relationship and Microstructural Requirements for Superplasticity

The mechanism of structural superplasticity has been established to be grain boundary sliding. The high temperature deformation based on grain boundary sliding can be represented by a generic constitutive relation (Nieh et al. 1997),

$$\dot{\varepsilon} = \frac{ADGb}{kT}\left(\frac{\sigma}{G}\right)^{n}\left(\frac{b}{d}\right)^{p} \tag{9.1}$$

where $\dot{\varepsilon}$ is strain rate, G shear modulus, b Burgers vector, σ applied stress, d grain diameter (size), D appropriate diffusivity, n stress exponent, p inverse grain size exponent, and A is a microstructure and mechanism dependent dimensionless constant.

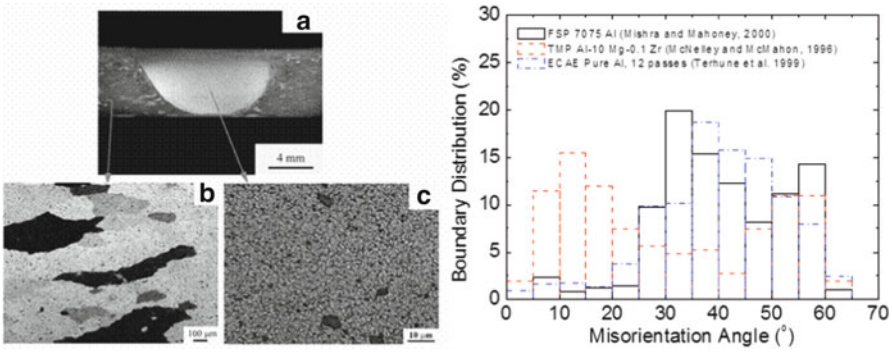

Fig. 9.3 Example of fine grain size in the friction stir processed nugget of Al7075 alloy. The grain boundary misorientation distribution shows the effectiveness of friction stir processing in producing high angle boundaries (Mishra and Mahoney 2007, reprinted with permission from ASM International)

Often in superplasticity literature, the strain rate sensitivity exponent ($m = \partial \log\sigma / \partial \log\dot{\varepsilon}$) is used instead of the stress exponent (n), shown in Eq. (9.1). However, 'm' is just the reciprocal of 'n'. Higher m values mean a greater resistance to external neck formation, and hence increased ductility. Generally, an m value of ~0.5 and a p value of 2–3 imply deformation by grain boundary sliding. The most important microstructural features that govern the overall superplastic behavior are:

(a) fine grain size (<15 μm),
(b) equiaxed grain shape,
(c) presence of very fine second phase particles to inhibit grain growth, and
(d) large fraction of high angle grain boundaries.

Friction stir process results in fine grain size and large fraction of high angle grain boundaries in aluminum alloys under a very wide range of processing conditions. Figure 9.3 shows grain refinement in Al7075 and a distribution of boundary misorientation. As mentioned in the initial chapters, because of large strain, high strain rate and high temperature, dynamically recrystallized microstructure with fine grain size evolves during friction stir process. It is typical to observe >90 % of grain boundaries with high misorientation (>15°). As discussed further, this microstructure is ideal for superplastic flow and forming.

9.1.2 Superplastic Flow in Friction Stir Processed Materials

In this section the examples of superplastic flow have been divided into conventional and non-conventional aluminum alloys. Conventional alloys are essentially commercial aluminum alloys that are readily available in various forms. In this context, a distinction between friction stir welding and friction stir processing needs to be made, particularly with regards to future possibilities. When friction stir welding is considered as a potential solution for an existing design of structure, it is important to keep

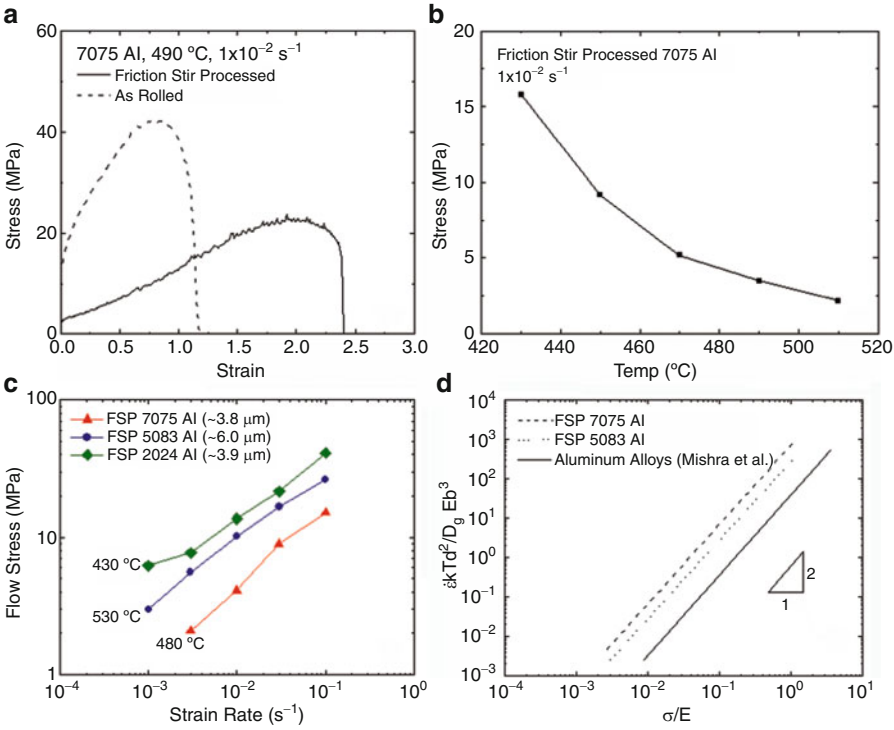

Fig. 9.4 (**a**) A comparison of flow curves for Al7075 alloy in as-rolled and as-FSP conditions at 10^{-2} s^{-1} strain rate. (**b**) The variation of flow stress data with temperature showing very low initial flow stresses. (**c**) A comparison of stress-strain rate behavior for three different commercial aluminum alloys. All of them show stress exponent close to 2 at the temperature selected. (**d**) A plot of normalized strain rate against normalized stress showing faster kinetics in FSP condition for both Al7075 and Al5083 alloy. For comparison a line for all conventionally processed aluminum alloys is included (Mishra and Mahoney 2007, reprinted with permission from ASM International)

the alloy selection same as original. On the other hand if a new system is being designed from ground up, and friction stir processing is a potential path, alloys with higher amount of dispersoids can be considered. In the examples presented in this section, Al-Zn-Mg-Sc and Al-Mg-Zr alloys are included. These are experimental alloys with considerable volume fraction of Al_3Sc and Al_3Zr, respectively, which effectively pins the grain boundaries at high temperatures for microstructural stability.

Figure 9.4 shows results for commercial aluminum alloys from three alloy series. The fine grained microstructure in friction stir processed condition leads to lower flow stress and much faster deformation kinetics. Figure 9.5 captures the variation of elongation with strain rate and temperature for these alloys. A remarkable part of this data set is the high strain rate range and wider temperature range over the superplasticity is observed. The comparison with as-rolled 6.3 mm thick rolled Al7075 alloy sheet is instructive in lack of superplasticity in sheets that are thicker and not particularly processed for superplasticity. So, fundamentally it highlights two limitations of conventional superplasticity; lower strain rate and

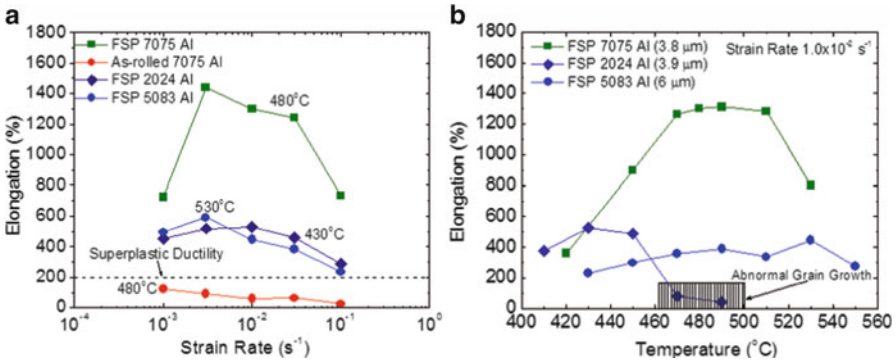

Fig. 9.5 Variation of elongation with (**a**) strain rate, and (**b**) temperature, showing high strain rate superplasticity

thinner sheets. In the plot against temperature, a region of abnormal grain growth is marked. This sets the upper limit for superplasticity in friction stir processed material. The abnormal grain growth aspect is different from conventionally processed aluminum alloys. It results from unique as-processed friction stir microstructure that contains strain gradients and microstructural gradients that can lead to microstructural instability at the higher end of temperature range.

Even better results are observed for unconventional aluminum alloys that contain very fine thermally stable second phase particles. Figure 9.6 shows results for two alloys containing Al_3Sc and Al_3Zr particles (Charit and Mishra 2005; Ma et al. 2010). An exceptional aspect of these results is that the peak elongation values are at strain rates higher than 10^{-2} s^{-1}, which is considered as the transition to high strain rate superplasticity. This has very important implications on total forming time and energy used in forming. Figure 9.7 adds additional information of grain size refinement to ultrafine region (<1 μm) in a single pass. The advantage of ultrafine grained microstructure is that the lowest temperature for high strain rate superplasticity drops to ~200 °C. This is still close to 0.6 T_m for this alloy. However, traditionally aluminum alloys do not show such low temperature superplasticity. Of course, the thermal stability at the higher temperature becomes an issue for such a fine microstructure. The main learning point from these results is that one needs to consider alloy chemistry, processing conditions, and design approaches in a holistic manner to take advantage of full potential of friction stir processing for superplasticity.

9.1.3 Friction Stir Processing as a Technology Enabler for New Concepts

This section is primarily taken from a previous review by Mishra and Mahoney (2007). Apart from the opportunity of achieving high strain rate superplasticity in commercial alloys, FSP offers several new opportunities as a 'technology enabler' (Mishra and Mahoney 2001; Mishra 2004; Mishra et al. 2004). Some of these possibilities are briefly described below (Mishra 2004).

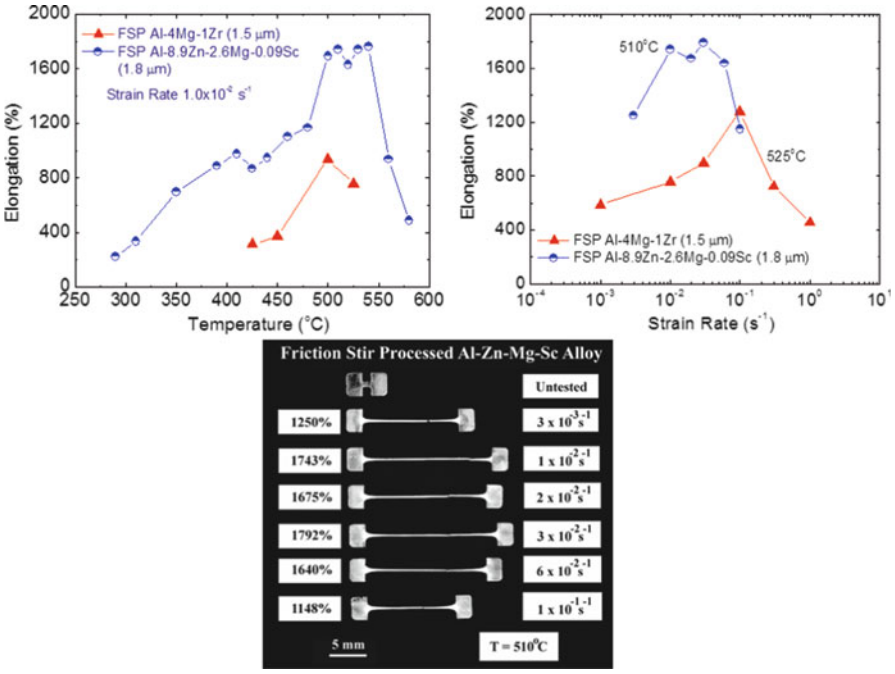

Fig. 9.6 Superplastic elongation data for two non-conventional aluminum alloys with very fine thermally stable particles. Note the peak elongation is at strain rate $>10^{-2}\ s^{-1}$, which is considered as transition to high strain rate

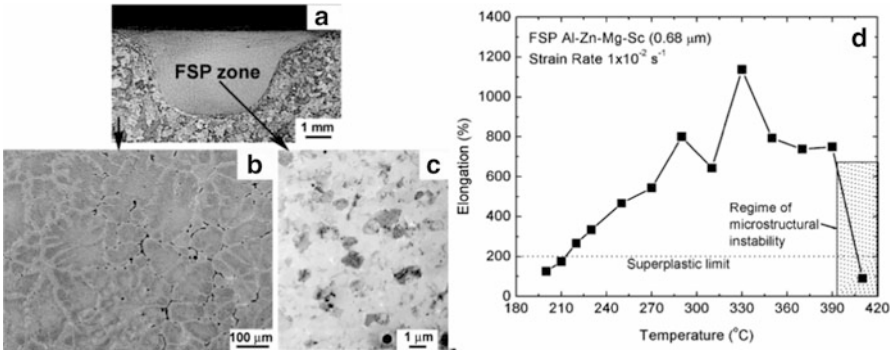

Fig. 9.7 Example of refinement of a cast Al-Zn-Mg-Sc alloy to ultrafine grained microstructure in one pass and associated high strain rate superplasticity at a very wide temperature range. Note the lower temperature limit of superplasticity. It also shows that the ultrafine grained microstructure limits the higher temperatures

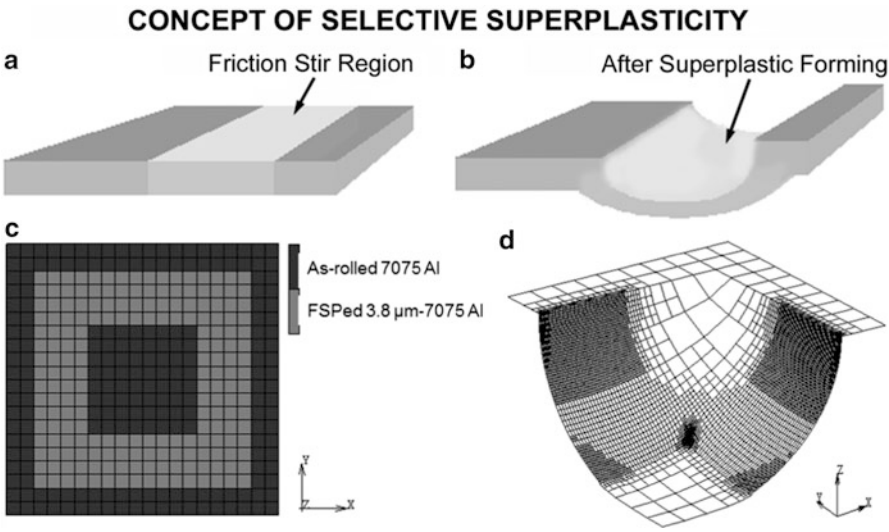

Fig. 9.8 (**a**) A schematic illustration of 'selective superplasticity,' where only the region undergoing superplastic deformation will be friction stir processed. (**b**) Brighter areas in the commercial 7075 Al rolled sheet are selected to be FSPed to become superplasticity instead of making the whole sheet superplastic. (**c**, **d**) Finite element mesh after adaptive remeshing (Wang and Mishra 2007, reprinted with permission from Elsevier)

9.1.3.1 Selective Superplastic Forming

In many components, only selected regions require superplastic deformation. The concept of such a superplastically formed component is shown in Fig. 9.8. In essence, only the region undergoing superplastic deformation needs the fine grained microstructure. However, conventional processing cannot be used to produce microstructural refinement on a 'selective' basis. FSP provides such an opportunity. Using FSP, a selected portion of the sheet can be processed for superplastic behavior. The difference in microstructure would result in selective deformation of the grain-refined region (Fig. 9.8). The FSP region with finer grain size undergoes superplastic deformation. This provides a versatile method to produce gas formed components with an intricate design.

9.1.3.2 Superplastic Forming of Thick Sheets

In conventional thermo-mechanical processing involving rolling of sheets, the sheet thickness reduces with every pass. To provide sufficient total strain for grain refinement, a number of passes are required resulting in thin sheets (<3 mm). On the other hand, when using FSP, the sheet thickness does not change. High strain rate and thick section superplasticity are two material properties never before demonstrated on a practical scale and are made possible only by FSP. For example, Mahoney et al. (2001) demonstrated high uniform elongation (>500 %) at strain rates

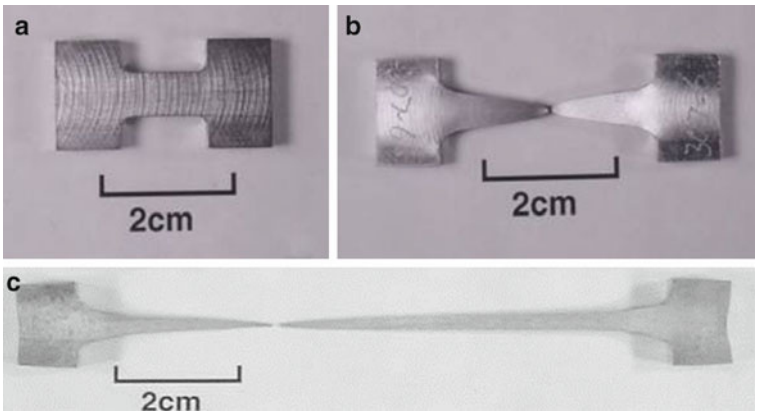

Fig. 9.9 (**a**) 5 mm thick tensile sample, (**b**) limited tensile elongation and severe necking without FSP, and (**c**) 800 % superplastic elongation in 5 mm thick FSP 7075 Al (Mishra and Mahoney 2007, reprinted with permission from ASM International)

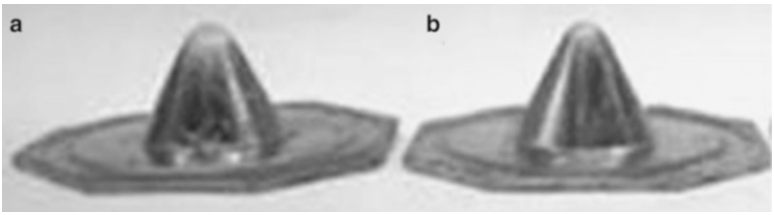

Fig. 9.10 Example of gas pressure cone tests for (**a**) a conventional superplastic 7475 Al alloy, 150 psi, 95 min, and (**b**) FSP 7475 Al 150 psi, 18 min (Mishra and Mahoney 2007, reprinted with permission from ASM International)

$>1 \times 10^{-3}$ s^{-1} at temperatures <460 °C. This offers the potential to form complex shaped parts at a higher strain rate and in section thickness never before possible. Figure 9.9 illustrates superplastic tensile elongation of ~800 % at 460 ºC following FSP in 5 mm thick FSP 7050 Al. The thickness limit for superplasticity has not been established but results up to 12 mm thick specimens have been published. Figure 9.10 shows cones formed by gas forming and make the important point of reduction in forming time. While a conventional superplastic 7475 Al alloy, i.e., the sheet was processed to a fine grain size (~15 μm grain size) via special thermomechanical processing, completely formed the cone at 150 psi in 95 min, the FSP 7475 Al (~3–4 μm grain size) completely formed the cone in a reduced time of 18 min. This type of reduction in forming time is exceptional from the energy saving point of view.

9.1.3.3 One Step Processing for Superplasticity from Cast Sheet or Hot-Pressed Powder Metallurgy Sheet

A conventionally cast microstructure can be converted to a superplastic microstructure in many steps. The present process of microstructural refinement can be

used directly on cast sheets. This leads to very economical manufacturing. Ma et al. (2004) have demonstrated superplasticity in A356 cast alloy. They were able to obtain a maximum superplastic elongation of 650 % at 530 °C for an initial strain rate of 1×10^{-3} s^{-1}. Charit and Mishra (2005) observed exceptional superplastic properties in an as-cast Al-8.9Zn-2.6 Mg-0.09Sc (wt%) alloy which is shown in Fig. 9.7. FSP with a smaller pin tool led to ultrafine grains (0.68 μm grain size) from the as-cast state. The ultrafine grained alloy exhibited superplasticity at relatively low temperatures and higher strain rates. An optimum ductility of 1,165 % at a strain rate of 3×10^{-2} s^{-1} and 310 °C was obtained. Enhanced superplasticity was also achieved at a temperature as low as 220 °C. A similar approach can be taken for direct chill cast or continuous cast sheet, thereby eliminating several steps. Similarly, powder metallurgy processed aluminum alloys require extensive thermomechanical processing to break down the prior particle boundaries that contain an alumina film. The friction stir process results in a very uniform microstructure from the hot pressed sheet. For example, FSP of a nanophase Al-Ti-Cu alloy results in a remarkable combination of high strength and ductility (Berbon et al. 2001). Again, the economical benefits of eliminating several steps are likely to be substantial. This approach will involve cast or PM sheet + FSP + SPF to produce high-strength, low-cost, unitized structures. These concepts can be applied to many metallic materials and metal matrix composites, but they have maximum impact on aluminum and magnesium alloys and components.

9.1.3.4 Superplastic Forming of Multisheet Structures

Multisheet structures are commercially fabricated by combining diffusion bonding and superplastic forming of titanium alloys. The key issue that helps titanium alloys and hinders aluminum alloys is diffusion bonding. Because of the surface oxide layer, diffusion bonding of aluminum alloys is difficult. This has limited the development of aluminum alloy multisheet structures. The work of Grant et al. (2006) has demonstrated the feasibility of making multisheet structures by combining FSW and FSSW with SPF. Figure 9.11 shows an example of a three-sheet structure created by FSW through two and three sheets. Fusion welding of aluminum alloys leads to a complete loss of superplasticity in the welded region because of microstructural changes. As noted earlier, the FSW microstructure consists of fine grains and superplastic properties are not degraded. A new opportunity involves microstructural tailoring by controlled heat input during FSW. The grain size can be varied by changing the thermal input. By controlling the microstructure, one can make the superplastic flow stress of the FSW region lower, higher, or equal to the parent sheet. Grant et al. (2006) have also used FSSW to create different types of multisheet structures. Their work is opening up new possibilities of sandwich structures using aluminum alloy sheets.

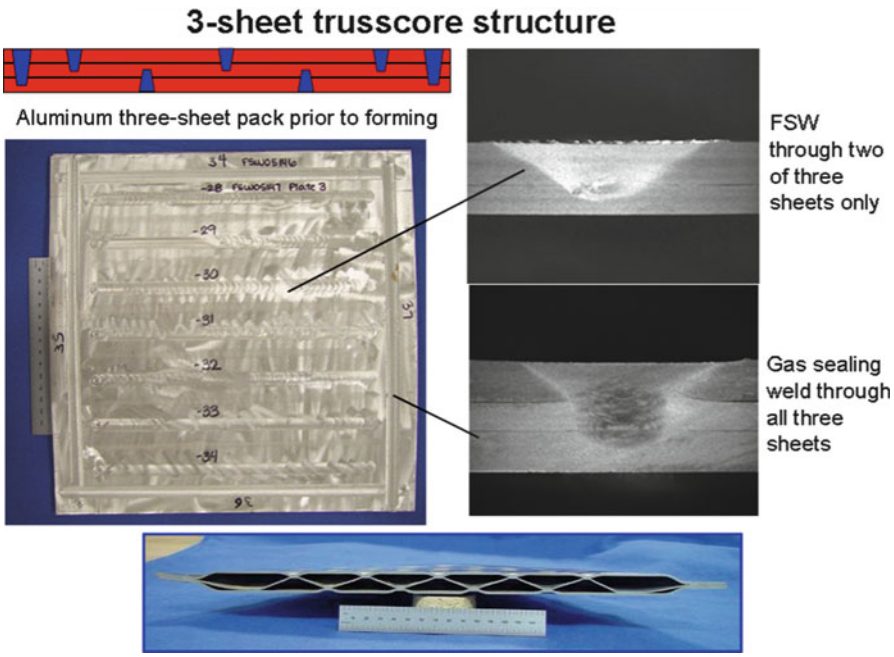

Fig. 9.11 An example of multisheet structure created by a combination of FSW and superplastic forming (figure courtesy Glenn Grant)

9.2 Enhanced Room Temperature Formability via FSP

Sheet metal forming is a very common technique for shaping of metallic components. An easy example is bending which is relatively simple operation. Smith and Mishra (2014) and Mishra and Mahoney (2007) have reviewed enhanced room temperature formability after friction stir processing. A relatively short discussion is presented to illustrate the potential of this approach. Datsko and Yang (1960) presented a very simple correlation between tensile properties and bending of a material as,

$$\frac{R}{t} = \frac{50}{A_r} - 1 \tag{9.2}$$

where R is the radius of bend (also referred as bend radius), t is the thickness of sheet/plate and A_r is the reduction of area during a tensile test. In this example, we just cover the basics with a solid solution strengthened aluminum alloy (Al 5083) and a precipitation strengthened alloy (Al 2519). The conventional tempers for Al 5083 aluminum alloys are O (annealed condition), F (as fabricated) and H (work hardened) tempers. The relevant temper for Al 2519 is T8 (solution treated, cold worked and artificially aged to peak hardness) and T3 (solution treated, cold worked and

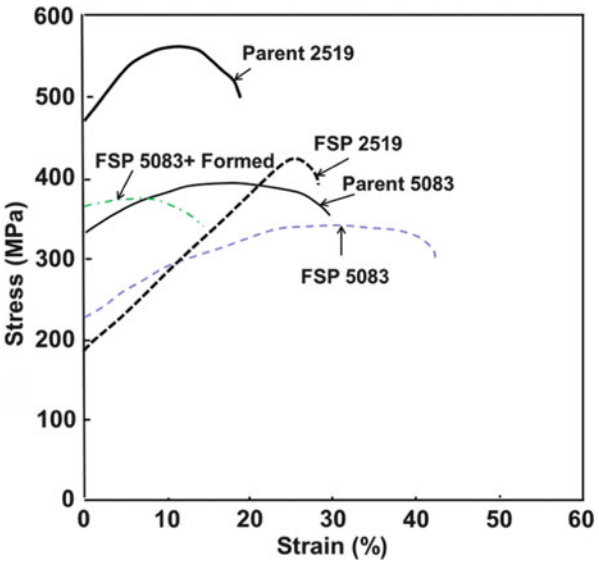

Fig. 9.12 Stress-strain curves for AA5083 and AA2519 in as-received and FSP conditions. Also, included is stress-strain curve of AA5083 specimen after FSP and room temperature bending

naturally aged to substantially stable condition). For friction stir processing, it is also important to consider definition of some other tempers that would not be conventionally used; T1 (cooled for elevated temperature shaping process and naturally aged to stable condition), T5 (cooled for elevated temperature shaping process and artificially aged).

Figure 9.12 shows stress-strain curves for AA5083 and AA2519 alloys. The AA5083 is a solid solution strengthened Al-Mg alloy. In this alloy, the relevant strengthening mechanisms are (a) solid solution strengthening, (b) dislocation storage based strain (or work) strengthening, and (c) grain boundary strengthening. The original material was in H temper and has high strength because of high retained dislocation density. FSP lowers the strength and increases the overall elongation. It is important to note that the net loss of strength reflects decrease in strength due to reduction in stored dislocation density and increase in strength due to grain refinement. After forming of such a solid solution strengthened alloy, the stored dislocation density increases. The stress-strain curve for AA5083 in formed condition reflects that. In the case of AA2519 alloy, the major strengthening component comes from Cu containing precipitates. The starting material for this alloy was in T8 temper. After friction stir processing the strength decreases and elongation increases because of the dissolution of precipitates in the nugget zone.

Figure 9.13 shows a cross-section of the friction stir processed region of AA5083 alloy after forming to an 8 mm (5/16″) internal radius. The bend axis was parallel to the rolling direction and centered about the FSP zone. However, one important note is the lack of any visible cracking, indicating the ability of FSP to locally enhance ductility, consistent with the stress-strain curve in Fig. 9.12. Little, if any, difference is noted in the macro cross-section other than obvious fact of the overall shape of the macro cross-section.

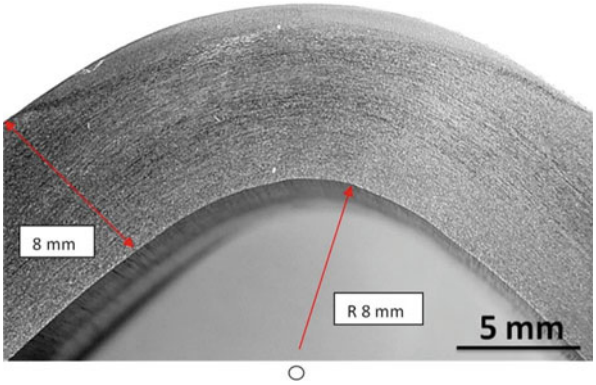

Fig. 9.13 A cross-section of the friction stir processed region of AA5083 after forming to an 8 mm (5/16″) internal radius (Smith and Mishra 2014, reprinted with permission from Elsevier)

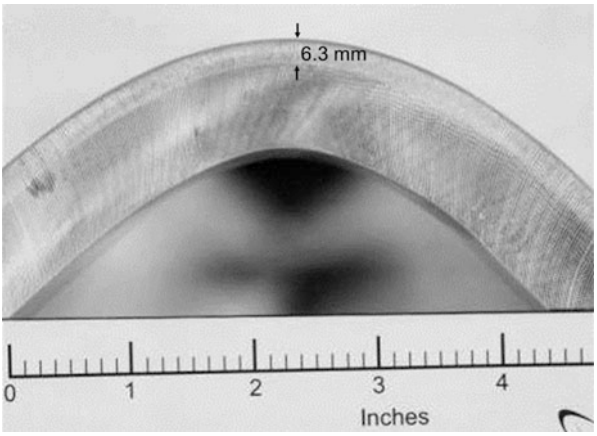

Fig. 9.14 Illustration of the FSP depth (6.3 mm) and the ability to bend 2519-T87 Al ~85° at room temperature (Mishra and Mahoney 2007, reprinted with permission from ASM International)

Figure 9.14 illustrates a transverse cross-section of the 25 mm thick 2519 Al plate following FSP to a depth of 6.3 mm. This depth was chosen somewhat arbitrarily and the same results may have been attained with less tool penetration. It demonstrates a concept of partial penetration friction stir processing of the surface experiencing tensile stresses during forming. The FSP zone is essentially annealed and below the FSP zone, there will be a heat affected zone (HAZ) with reduced mechanical properties. The sample shown in Fig. 9.14 has been bent 85° (limit of the die) at room temperature without any indication of impending failure.

The examples shown so far in the chapter showed enhanced formability of material due to microstructural refinement and modification. In Fig. 9.2, five design limited approaches are listed, namely, stiffness limiting, strength limiting, fatigue

limiting, toughness limiting and creep limiting. The next two sections deal with localized microstructural modification to deal with some of these design approaches.

9.3 Friction Stir Processing of Surface Composites and Powder Processing: Approach for Stiffness Limiting Design

Metal matrix composites (MMCs) are used because they allow combinations of the properties of metals and ceramics. Compared to unreinforced metals, metal-matrix composites reinforced with ceramic phases exhibit high strength, high elastic modulus, and improved resistance to wear, creep and fatigue. For example, the modulus of a metal can be increased by adding ceramic particulates (or fibers or whiskers). Typically ceramics have much higher moduli than metals and a combination of the two can lead to composites with tailored values of the modulus. Materials with higher moduli are desirable for components that are designed for high stiffness. The guiding principle for these composites for density and modulus has been the rule of mixtures (Ashby 2003),

$$P_{comp} = fP_r + (1 - f)P_m \tag{9.3}$$

where P represents property of interest (density or modulus), f is the volume fraction of reinforcement, and subscripts comp, r and m denote composite, reinforcement and matrix, respectively. The theoretical prediction based on the rule of mixture, gives an upper estimate of the property that can be obtained. Although a more precise limit can be predicted (Eshelby 1957; Hashin and Strikman 1962), these values are always lower than that predicted by the rule of mixtures. Therefore, for the purposes of this chapter, Eq. (9.3) can be used to benchmark for further discussion and will be referred to as 100 % of the predicted value.

The enhanced properties make MMCs promising structural materials for the aerospace and automobile industries. However, MMCs also suffer from a great loss in ductility and toughness due to incorporation of non-deformable ceramic reinforcements, and are relatively costly. These restrictions limit their wider utilization. For many applications, the useful life of components often depends on surface properties such as wear-resistance. In these situations, only the surface layer needs to be reinforced by ceramic phases while the bulk of the component could retain the original composition and structure with higher toughness. There is also an emphasis on added functionality. For example, a structural component can be designed to serve additional non-structural functions. This approach has the possibility of integrating subsystems.

Table 9.1 Some examples of properties that can be tailored by localized surface modification (Mishra and Mahoney 2007, reprinted with permission from ASM International)

Property	Approach
Elastic modulus	Addition of ceramic particles or intermetallic particles
Wear resistance	Addition of second phase particles and microstructural refinement can enhance wear properties
Fatigue	Addition of shape memory particles can alter the residual stresses, thereby influencing the fatigue properties
Magnetic	Magnetic particles can be added in local regions to obtain magnetic properties in otherwise non-magnetic materials
Electrical conductivity	Second phase additions can be used to enhance or lower the electrical conductivity
Thermal conductivity	Second phase particles can be used to enhance or lower thermal conductivity based on the thermal conductivity of matrix and reinforcement
Damping	Shape memory particles and piezoelectric particles can be added to enhance the damping capabilities

9.3.1 Localized Surface Modification

Localized surface modifications can be a very powerful tool to achieve the right combination of properties, i.e., a gradient of properties within a monolithic structure. The potential exists to broaden design possibilities using metal matrix composites surfaces. Some examples of properties that can be influenced are listed in Table 9.1. A number of these approaches require particles of a stoichiometric nature. The properties of these particles can degrade or change if they undergo chemical reaction with the matrix. The short thermal cycle and relatively low temperature during FSP can help to avoid or eliminate reaction products. This is a key distinction compared to other techniques like laser processing that involves melting of matrix phase. Some examples from early efforts are summarized in Table 9.2 to illustrate the range of particles and phases that can be added. The second phase particles can be added in various geometrical configurations. Figure 9.15 gives a few simple examples, but a variety of combinations are possible and have been reported in literature. There are two aspects: (a) type of addition configuration, and (b) frequency. The shape, size and frequency of these features control how much second phase can be added. This interacts with the tool pin features in terms of nugget cross-section. Both combined together control the volume fraction in the embedded region. Each method has some inhomogeneity associated with it. A pre-processed strip would be good, but it adds to number of steps.

Figure 9.16a, b show examples of SiC distributed using the surface addition method (Mishra et al. 2003; Ma et al. 2003). The uniform SiC distribution is demonstrated and a reaction and defect free composite/matrix interface illustrated. Figure 9.16c shows the fracture surface of a single wall carbon nanotube-aluminum composite tested in tension (Johannes et al. 2006). The survivability following large processing strains and the thermal cycle is noteworthy. This illustrates the

Table 9.2 A summary of some examples of surface modification and in-situ composite efforts (Mishra and Mahoney 2007, reprinted with permission from ASM International)

Material system	Remarks
5083 Al-SiC (Mishra et al. 2003)	SiC particles were put on the surface and stirred into the matrix
A356 Al-SiC (Ma et al. 2003)	SiC particles were put on surface and stirred into the matrix
7050 Al-WC (Newkirk et al. 2003)	WC particles were put a machined surface slot and stirred
1100 Al-SiO_2 and TiO_2 (Howard et al. 2005)	Introduced the concept of reaction processing during FSP. The reaction product was placed sub-surface with a three-layer set-up and friction stir processed
7050 Al and 6061 Al-WC, SiC, Al_2O_3, MoS_2, Fe, Zn, Cu (Ramadorai et al. 2005)	Powders were placed in sub-surface drilled holes. The hole geometry provided good control of the volume fraction. A number of ceramic and metallic phases were explored, including a combination of SiC and MoS_2
AZ61-SiO_2 (Lee et al. 2006a, b)	Distributed nano-particles by using repeated runs
Al-SWCNT (Johannes et al. 2006)	Demonstrated the survivability of single wall carbon nanotubes (SWCNT) during FSP. The nanotubes were placed sub-surface by drilling a hole from top and using a plug
AZ31-MWCNT (Morisada et al. 2006)	Multi-wall carbon nanotubes (MWCNT) were distributed in a Mg alloy
Al-NiTi (Dixit et al. 2007)	Shape memory alloy (NiTi) was distributed using the hole method without any interfacial reaction with Al

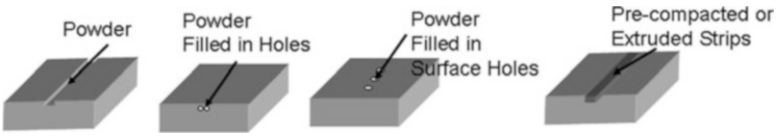

Fig. 9.15 An illustration of a few ways of adding powder during FSP surface modification. Note that all approaches lead to some inhomogeneity

possibility of developing sensors and actuators by locally embedding functional particles. In another attempt to embed functional particles, Dixit et al. (2007) have observed clean Al-NiTi interfaces after friction stir processing (Fig. 9.16d).

9.3.2 Processing of Powder Metallurgy Alloys

Powder metallurgy processed aluminum alloys suffer from three major microstructural problems that limit their full potential: (a) prior particle boundaries with an aluminum oxide film, (b) microstructural inhomogeneity, and (c) remnant porosity. These microstructural features particularly hamper the ductility in very high strength

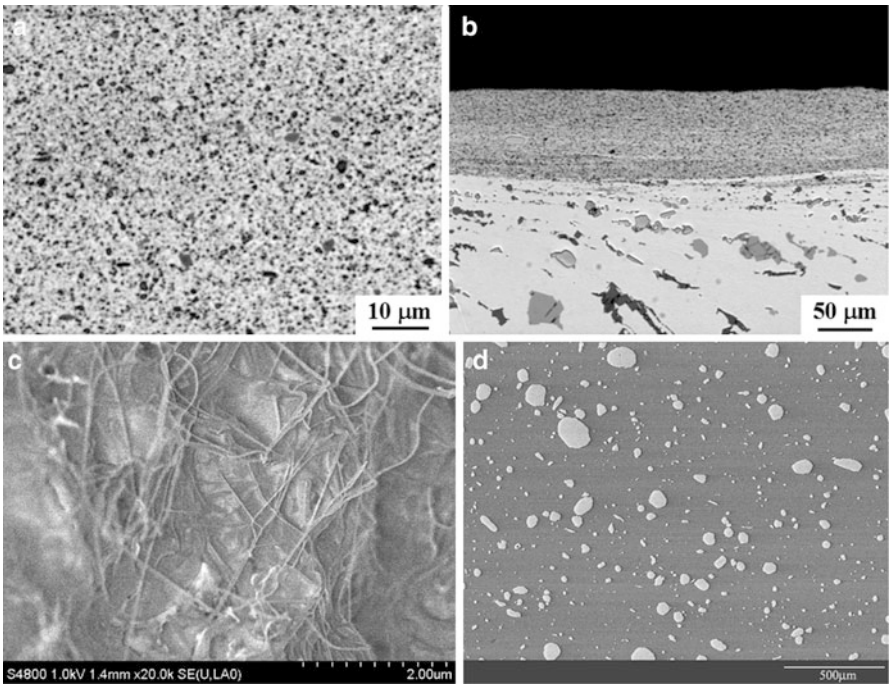

Fig. 9.16 Optical micrograph showing (**a**) uniform distribution of SiC particles (~15 vol.%) in A356 matrix, and (**b**) perfect bonding between surface composite and aluminum alloy substrate (600 rpm rotation rate and 6.4 mm/min traverse speed) (Ma et al. 2003). (**c**) SEM image showing SWCNTs bundles on the fracture surface of a friction stir processed aluminum matrix (Johannes et al. 2006). (**d**) SEM image showing uniformly distributed NiTi particles in Al matrix (Dixit et al. 2007) (Mishra and Mahoney 2007, reprinted with permission from ASM International)

aluminum alloys. Berbon et al. (2001) and Zheng et al. (2001) have shown that FSP can be used a homogenization tool. Figure 9.17 shows the microstructural difference in an Al-Ti-Cu alloy processed by extrusion and by FSP. The FSP microstructure is remarkably different from the as-extruded microstructure. This leads to an excellent combination of strength and ductility. Spowart et al. (2003) have highlighted the effect of spatial heterogeneity on mechanical properties. They used FSP to modify the homogeneity of three aluminum matrix composites produced with controlled inhomogeneity. Figure 9.18 shows the relationship between homogeneous length scale and ductility in aluminum matrix composites. Results clearly demonstrate that FSP can be a very useful tool to enhance the mechanical properties of high strength alloys and composites. Combining the trends observed by various studies cited in this section, the potential of FSP as a tool to create homogeneous composites on a local scale can be visualized. Designers and fabricators can take this approach to design components and sub-systems to take advantage of localized property enhancements to augment conceptual design elements.

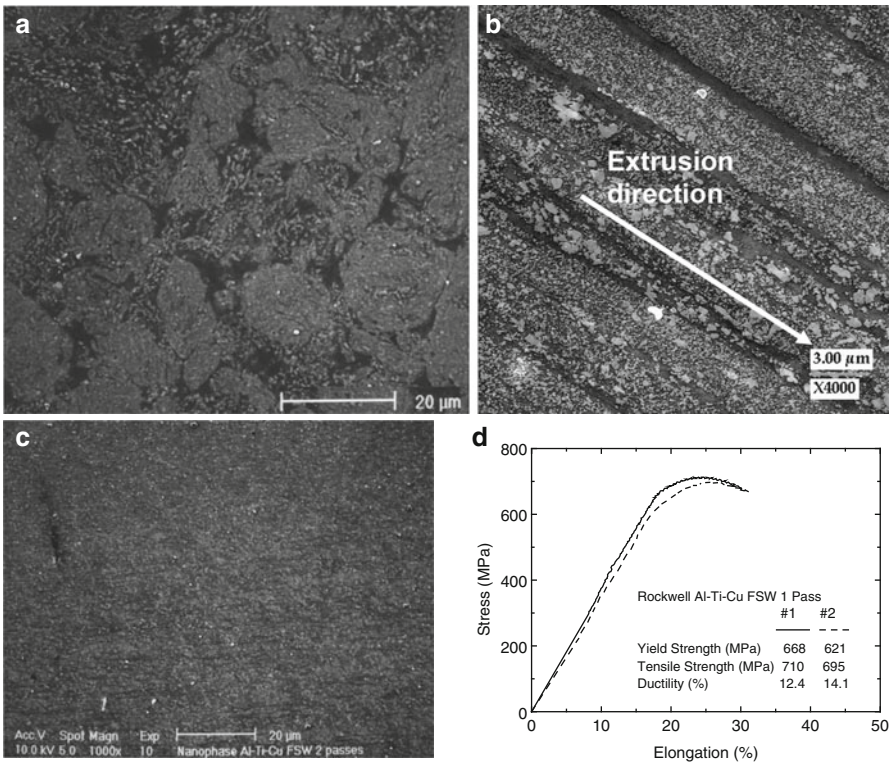

Fig. 9.17 (**a**) Typical microstructure in the as-HIPed condition. Dark regions consist of pure Al, grey regions consist of fine intermetallics dispersed in an Al matrix, and light regions consist of coarse intermetallics in an Al matrix. (**b**) Typical as-extruded microstructure shows the same three microstructural features, now elongated in the extrusion direction. (**c**) Typical microstructure observed in the FSP nugget. The three different microstructural features seen in the starting material have been homogenized. (**d**) Tensile tests of the Friction Stir processed material show an excellent strength and more than 10 % ductility (Berbon et al. 2001) (Mishra and Mahoney 2007, reprinted with permission from ASM International)

9.3.3 Synergistic Design: Concept of Embedded Structures for Higher Efficiency

This concept has two aspects to it. The first one is a generic concept dealing with the question: Can more than 100 % structural efficiency be obtained by synergistic design of composites? In what follows, it is argued that it is possible to combine two design features, volume fraction of reinforcement and location of reinforcement, to obtain synergistic enhancement that leads to >100 % efficiency. The second aspect relates to economical manufacturing of such composites. FSP has the potential to provide such a processing route.

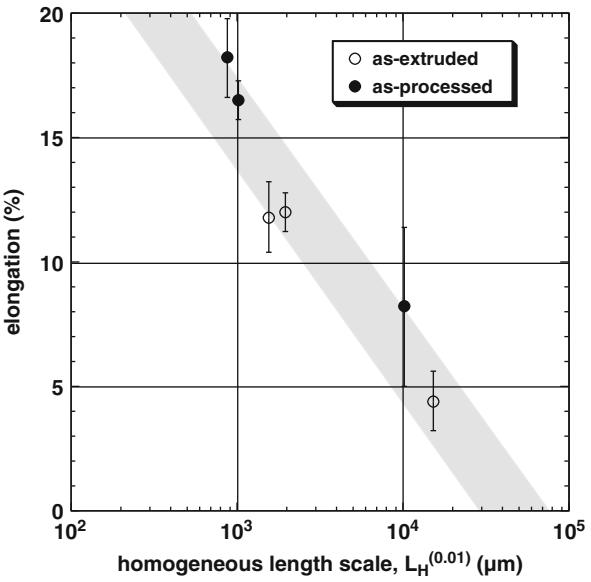

Fig. 9.18 A relationship between tensile elongation and level of spatial heterogeneity, as characterized by the homogeneous length scale, $L_H^{(0.01)}$ (Spowart et al. 2003)

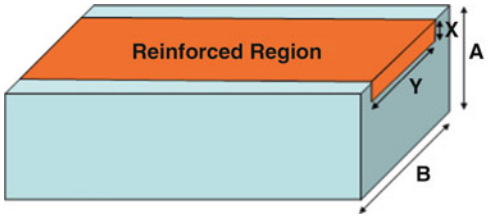

Fig. 9.19 An illustration of the concept of selective reinforcement for synergistic enhancement

Figure 9.19 illustrates the concept of selective reinforcement. The idea of synergistic enhancement is based on interaction between two length scales of materials design. At the microstructural level, mixing of two phases will lead to property enhancement following the rule of mixture. At the meso or macro-scale, the product can be designed to maximize the property at strategic locations. To illustrate this concept we select stiffness as an example, although a similar strategy will work for several other properties as well. In Fig. 9.19, the overall cross section of the beam is A × B. For the selectively reinforced concept, only the region with cross-section of X × Y has particles. For this design two other considerations can be brought in, (a) during bending of beams, the stresses are maximum at the surface and go through the neutral axis in the center, and (b) metal matrix composites suffer from poor tensile ductility, but have excellent compressive properties. If we want to have 30 vol.% reinforcement in this region for a specific level of stiffness of the beam, it can be put on the compressive side of the beam. The equivalent volume fraction of particles in a monolithic composite (material with uniform distribution of particles) can be computed as $0.3 \times \{(X \times Y)/(A \times B)\}$. If we now apply a force

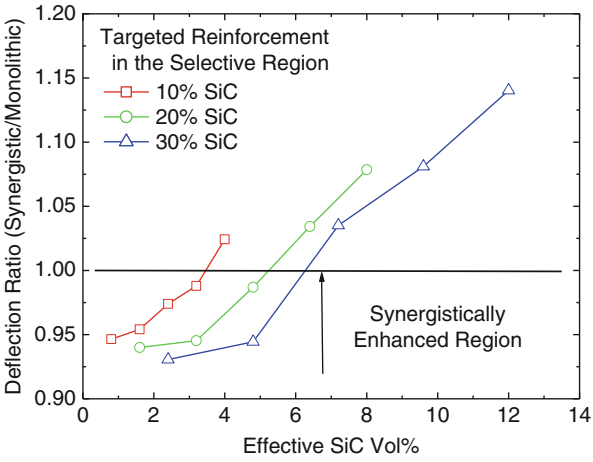

Fig. 9.20 Enhancement in stiffness results from synergistic design (Tandon and Mishra, unpublished)

Table 9.3 Summary of equivalent vol.% SiC in monolithic beam for different depth of selectively reinforced layer

Vol.% of SiC in selective region	Reinforced layer depth—X (mm)				
	0.5	1.0	1.5	2.0	2.5
10	0.8	1.6	2.4	3.2	4.0
20	1.6	3.2	4.8	6.4	8.0
30	2.4	4.8	7.2	9.6	12.0

on these beams with different designs, but an equivalent overall reinforcement phase, the level of deflection would indicate the effectiveness of the design. It should also be recognized that poor bonding between the reinforcement phase and matrix lowers the load transfer and therefore leads to lower stiffness.

Figure 9.20 shows the efficiency of synergistic design. Three curves are presented for different volume fractions of SiC in the selective region of an AA5083 beam. The following dimensions of the beam and selective layers were used: A = 5 mm; B = 10 mm; Y = 8 mm. Table 9.3 shows the equivalent SiC fraction in a monolithic composite beam given the mixed beam composite's strip fraction of SiC and the strip depth. The value of X was varied between 0.5 and 2.5 mm. It is very interesting to note that the best results are obtained for thin selectively reinforced region. In fact when the depth is such that it touches the neutral line (center of beam), the selectively reinforced composite is worse than the monolithic beam (uniformly reinforced beam). This is an important factor to consider on component design. The enhancement for thinner layers can be as much as 7 %. The implication is that for the same design stiffness, up to 7 % weight saving can result from synergistic design within the range considered here. Further improvement can be obtained by optimizing the modulus and density of the reinforcement phase.

9.4 Friction Stir Casting Modification: Examples of Approaches for Strength Limiting, Fatigue Limiting and Toughness Limiting Designs

Casting is the most cost efficient way to produce complex shaped parts. However, castings suffer from many microstructural issues that limit its performance. Forging on the other hand is a preferred manufacturing technique for high performance components. The basic difference of course lies in the microstructure; wrought microstructure in forgings vs. solidification microstructure in castings. So, the paradigm shift that friction stir processing offers is to have 'wrought microstructure in localized regions of a cast component'; a balance between cost, complexity and performance of a component. Critical microstructural features in a casting can be listed as,

- Large oxide films
- Large dendritic porosity (larger than 1 mm)
- Small dendritic porosity (smaller than 1 mm)
- Particulate oxides/inclusions
- Secondary dendritic arm spacing (SDAS). The high stress regions are frequently the slowest to solidify, with larger SDAS.
- Silicon modification and iron-phase intermetallics
- Non-dendritic (~spherical) hydrogen gas porosity

Conventional approach in casting is to increase the cross-section of high stress regions. This leads to lower cooling rate in those areas and the microstructure is actually inferior in the critical regions. Rest of this section shows examples of friction stir processing induced microstructural refinement and its influence on strength, ductility, fatigue and toughness.

9.4.1 Microstructural Refinement

Figure 9.21 shows a comparison of cast and friction stir processed microstructure for three commercially cast components of A356 alloy. The level of porosity and dendritic arm spacing is different in all the specimens. Also the particles in interdendritic regions have different sizes because of the practice of adding Si modifier. After friction stir processing, the obvious microstructural changes include, elimination of porosity, refinement of particles and homogenization of microstructure. The effect of FSP on particle size can be quantitatively seen from distribution histograms shown in Fig. 9.22. It is important to focus on the larger particles. In as-cast condition, more than 10 % particles are above 15 μm. During mechanical loading such as tensile test or fatigue test, larger particles are the local area where failure starts. Table 9.4 summarizes the microstructural refinement and changes in the context of critical features in castings discussed above. It reemphasizes the refinement of particles, homogenization of microstructure and elimination of porosity.

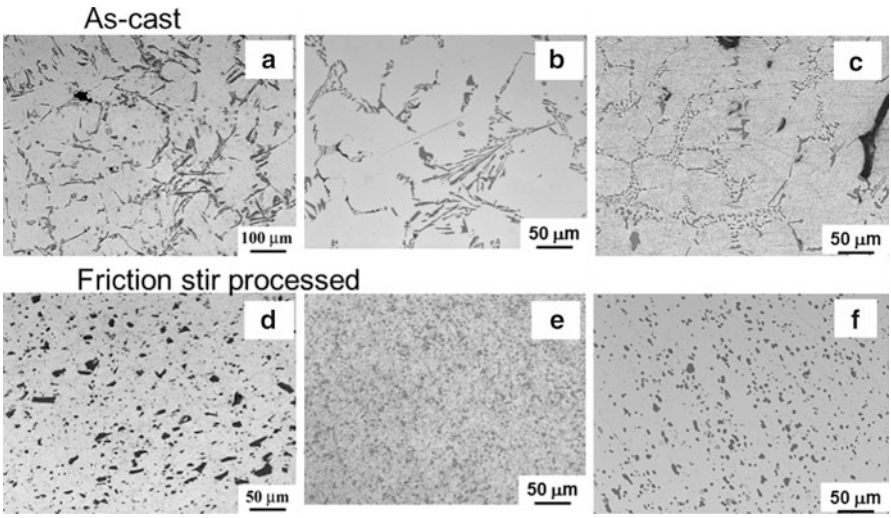

Fig. 9.21 A comparison of as-cast (**a**, **b**, **c**) and friction stir processed (**d**, **e**, **f**) microstructures of A356 alloy from three commercial casting. Note the dendritic arm spacing, large particles and porosity in as-cast condition. FSP refines and homogenizes the microstructure as well close all the porosity

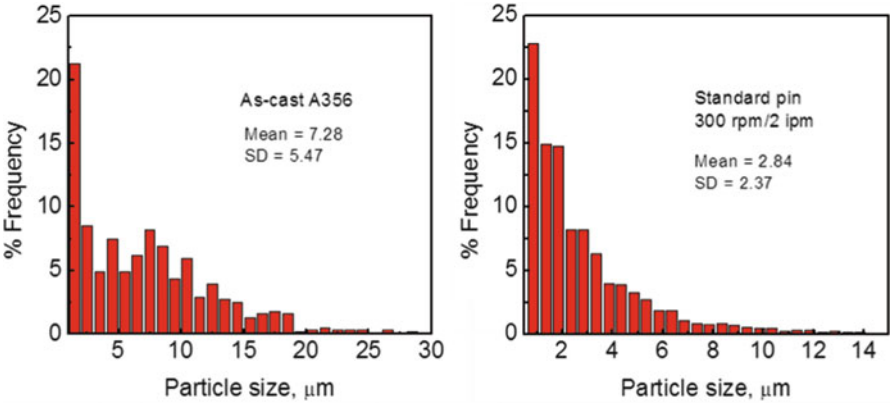

Fig. 9.22 Distribution of particle size in as-cast and after FSP for A356 alloy in one cast condition. Note the reduction in maximum particle size. More than 10 % of particles in as-cast condition were above 15 μm

A206 is an Al-Cu casting alloy that is capable of much higher strength levels, but suffers from higher level of porosity. Figure 9.23 shows microstructure of A206 alloy before and after FSP. The strengthening phase in this alloy is Al_2Cu. The microstructural summary after refinement is listed in Table 9.5. The volume fraction of large particles in this alloy is significantly lower than A356, but the size of coarser phase is quite similar.

Table 9.4 A summary of the influence of FSP on critical microstructural features

	As-cast A356	Friction stir processed
Porosity	0.005–0.03 %	Almost 0 %
Fe rich intermetallics	11.1 mm	3.0 mm
Si size	3.6 mm	1.0 mm
Si aspect ratio	2–7	1–2
Oxide inclusion	Non-uniform	Fine and distributed
Homogenize	No	Yes

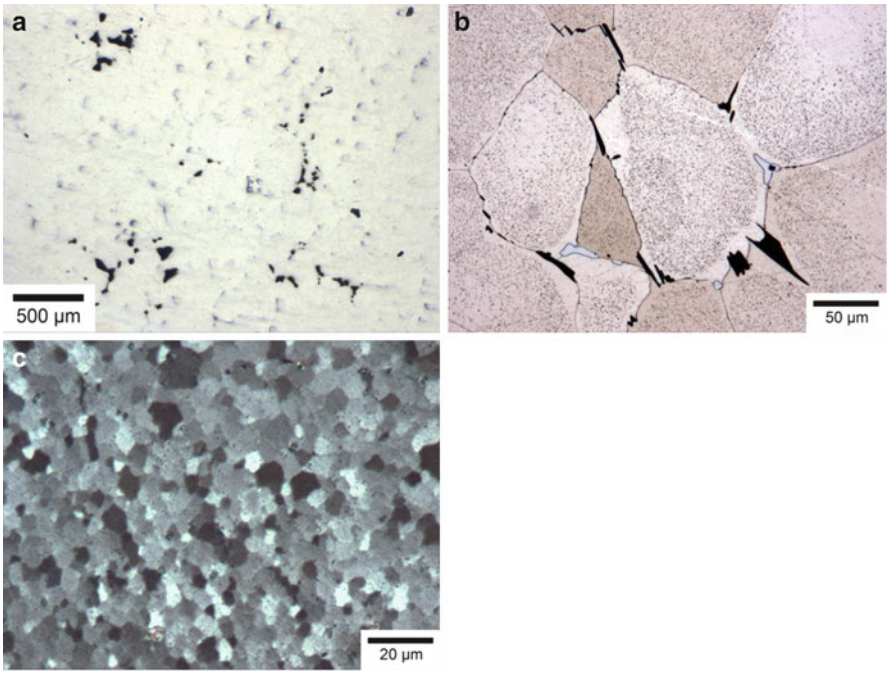

Fig. 9.23 Optical microscopy of A206 in cast + T4 condition showing pores (**a**), needle shaped Cu_2FeAl_7 intermetallics (**b**), and grain distribution after FSP (**c**) (Kapoor et al. 2011, reprinted with permission from Elsevier)

Table 9.5 Comparison of microstructural features, pores, particles, grains and precipitates in different heat treatment conditions

Name	Pores (μm)	Particles (μm)	Grains (μm)	Precipitates
Cast + T4	14.7 ± 2	5.6 ± 2.5	210 ± 6	Coherent
As-FSP	None	2.9 ± 1.4	3.5 ± 1.5	Coherent
FSP + 190C	None	2.9 ± 1.4	3.5 ± 1.5	Incoherent
FSP + T4	None	2.9 ± 1.4	350 ± 200	Coherent
FSP + T6	None	2.9 ± 1.4	350 ± 200	Semi-coherent
FSP + T7	None	2.9 ± 1.4	350 ± 200	Incoherent

The average values with standard deviation for pores, particles and grains are listed along with the type of precipitates present in the different conditions (Kapoor et al. 2013, reprinted with permission from Elsevier)

Table 9.6 A summary of A356 room temperature tensile properties from an average of five specimens. The differences between Cast+T6 and FSP+T6 are highlighted

Condition	UTS (MPa)	YS (MPa)	% E
As cast (handbook)	159	84	6
Cast + T6 (handbook)	278	207	6
Cast	169 ± 8	132 ± 3	3 ± 1
Cast + T6	$\mathbf{231 \pm 30}$	$\mathbf{225 \pm 20}$	$\mathbf{0.6 \pm 0.4}$
Cast + FSP	264 ± 3	168 ± 9	13 ± 2
Homogenized + FSP	262 ± 7	168 ± 4	12 ± 2
T6 + FSP	228 ± 9	144 ± 7	14 ± 4
FSP + T6	$\mathbf{328 \pm 12}$	$\mathbf{288 \pm 9}$	$\mathbf{10 \pm 1}$
Homogenized + FSP + Aged	311 ± 15	277 ± 17	4 ± 1

9.4.2 Influence on Mechanical Properties

9.4.2.1 Tensile Behavior

A number of papers have reported mechanical behavior of castings before and after FSP. We focus on only a few results which are adequate to illustrate the point. A356 and A357 are very popular Al-Si-Mg alloys which have Si for fluidity and Mg_2Si precipitates for strengthening. Table 9.6 gives one set of data from sand cast A356 alloy. It is important to focus on both the average values and the standard deviation. As the components are designed to some minimum guaranteed property value, we can take (Mean YS-3σ) values in cast + T6 (165 MPa) and FSP + T6 conditions (261 MPa). This represents nearly 58 % increase in the design stress if the design guideline is based on yield strength. This table also shows various pathways for insertion of FSP. For example, a typical production of cast component involves; casting, homogenization and aging, then final machining. A question that comes up is on insertion of FSP step. What is the most prudent stage to do it? Based on the basic value addition proposition, one can think of many pathways. Let us discuss a few scenarios. Bear in mind that all the discussion is based on the premise that casting modification would be done in local regions where in the current context, higher strength or higher fatigue life is desired. The selection of the region is based on some form of stress analysis, say finite element modeling of the entire component. The most conservative approach would be to insert it after homogenization and perform T6 treatment after FSP. The machining would still be the last step. A paradigm changing approach would be to declare that FSP takes care of homogenization and solution treatment. Then the production can be simplified to casting, FSP and aging. This would result in significant energy saving associated with homogenization and solution treatment. Of course, several other paths in between these two limits can be used to insert FSP step in production.

A206 alloy is an Al-Cu casting alloy that is significantly stronger. Kapoor et al. (2013) have published detailed tensile behavior in many conditions. Figure 9.24 shows stress-strain curves as well as summary of strength-ductility variation.

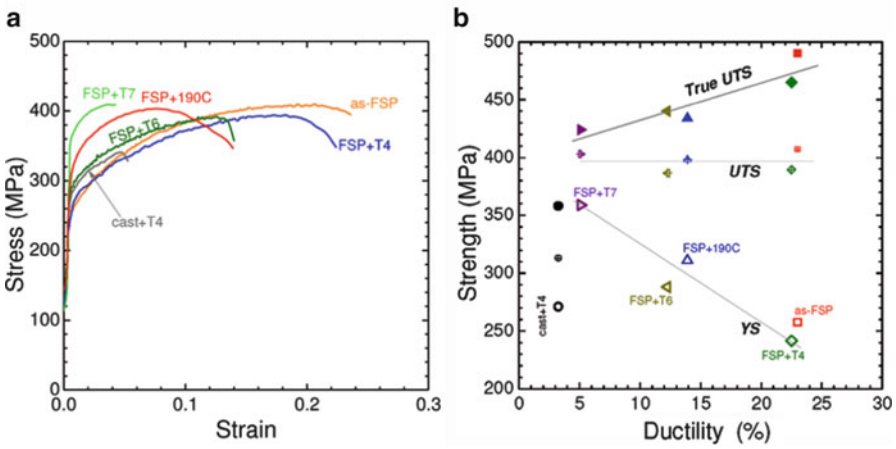

Fig. 9.24 (**a**) Stress-strain plot for A206 alloy in different conditions. The strength and ductility data from these curves is plotted in (**b**). Note that while engineering UTS values are constant for various FSP specimens, the true UTS values are higher for specimens with higher ductility. Kapoor et al. (2013), reprinted with permission from Elsevier

There are several interesting trends in this. This alloy is similar to 2XXX alloys in wrought condition unlike A356 alloy, which has no equivalent wrought composition. So, the first aspect that needs comparison is the strength level. The yield strength after FSP and aging is in the range of 350 MPa and UTS values are around 400 MPa. These values are very consistent with AA2XXX alloys. The yield strength-ductility relationship has a typical profile of structural materials, i.e. the ductility decreases as the strength increases. However, an interesting aspect is that the engineering values of UTS are constant. When plotted as true UTS vs. ductility, it shows that FSP and FSP + T4 specimens which have lower yield strength show highest UTS because of high strain hardening as high uniform elongation.

The casting industry uses strength and ductility data to define 'quality index'. Drouzy et al. (1980) have proposed a simple relationship to represent quality index (Q) as,

$$Q = \sigma_{UTS} + 150 \log E \tag{9.4}$$

where σ_{UTS} is the ultimate tensile strength and E is the elongation. Figure 9.25 shows a quality index plot for A356 alloy that was discussed earlier. The improvement in Weibull modulus after FSP is quite obvious and this suggests high reliability after FSP.

9.4.2.2 Fatigue Behavior

A number of fatigue behavior papers have been published on friction stir processing of aluminum and titanium alloys, but we focus on just a few to lay out the basic foundation behind the improved fatigue behavior. Figure 9.26 illustrates fatigue

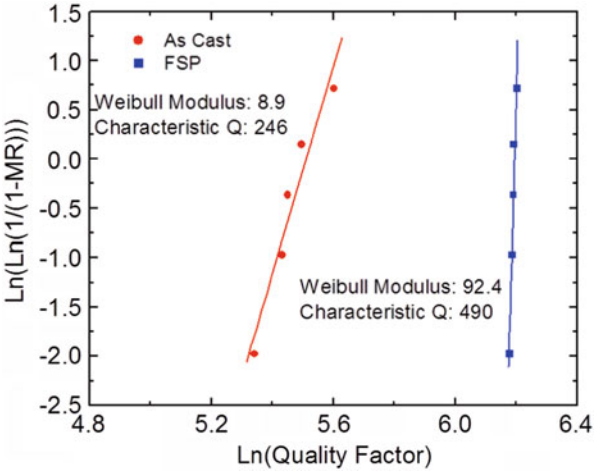

Fig. 9.25 A plot of quality index showing significant in Weibull modulus after friction stir processing of A356 alloy

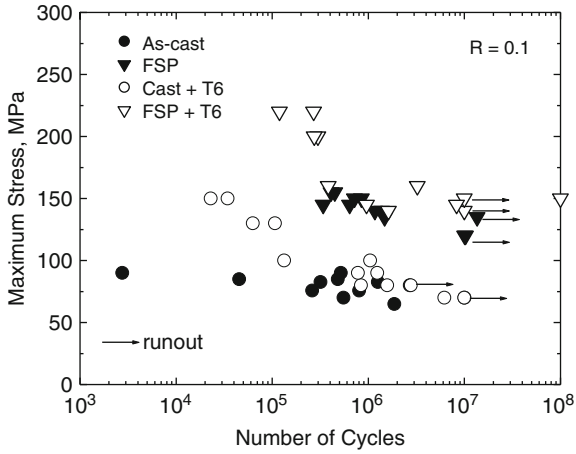

Fig. 9.26 Plot of fatigue lifetime vs. maximum stress for as-cast and FSP A356 samples (Sharma et al. 2004, reprinted with permission from Elsevier)

results for A356 plates before and after FSP (Sharma et al. 2004). For processed plates, the samples were machined completely from the stir zone. The arrows in Fig. 9.26 indicate specimens that did not fail. As shown, the fatigue strength threshold stress increased by >80 % after FSP. This fatigue strength improvement is attributed to both a reduction in silicon particle size and reduced porosity volume fraction. The fatigue life N_f has been related to the positive component of cyclic stress, σ*, and the pore size a_o, by:

$$\sigma^* = C\left(a_o N_f\right)^{-\frac{1}{m}} \tag{9.5}$$

where m is the Paris exponent for fatigue crack growth and C is a constant that depends on the Paris pre-exponential constant and on the pore shape and position. From the above analysis, it was concluded that fatigue life is influenced more by the

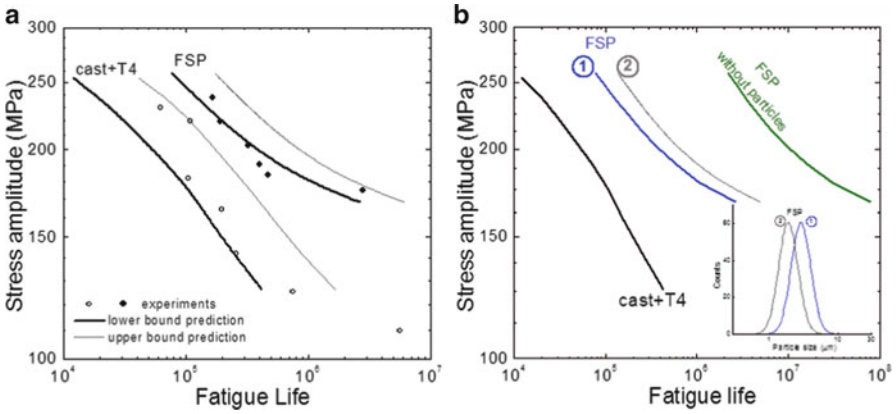

Fig. 9.27 (**a**) A comparison between the experimental and predicted stress amplitude vs. fatigue life for both cast + T4 and FSP conditions. The lower and upper bounds of the prediction are shown on the plot. (**b**) Stress amplitude vs. lower bound of computed fatigue life showing cast + T4 and FSP conditions from actual defect distribution labeled 1. Also shown is the predicted lower bound of life for distribution of smaller particles labeled 2 and the predicted lower bound of life for a condition without particles. The *inset* shows the corresponding particle distribution marked as 1 and 2. (Kapoor et al. 2011, reprinted with permission from Elsevier)

size of the largest pore rather than porosity volume fraction or mean pore size. In addition to porosity, fracture characteristics of Al-Si-Mg castings are influenced by size, orientation and local distribution of Si particles as well as by the Si-matrix interface strength. Larger Si particles present in the as-cast material accelerate crack nucleation due to stress concentration effects. Murakami and Endo (1994) have proposed the following equation for the fatigue limit in metals with 3-D defects:

$$\sigma_w = \frac{1.43(H_V + 120)}{(\sqrt{A})^{\frac{1}{6}}} \tag{9.6}$$

where σ_w is the fatigue limit (MPa), A is the area obtained by projecting a defect or a crack onto the plate perpendicular to the maximum tensile stress (mm), and H_v is Vickers hardness (kgf mm^{-2}) between 70 and 720 H_v. Based on Eq. (9.6), a 30 % reduction is particle size alone would contribute to a 25 % improvement in the fatigue limit. FSP significantly refines the microstructure leading to a homogeneous distribution of smaller Si particles with smaller aspect ratios when compared to the as-cast microstructure. This refined microstructure also leads to increased plastic deformation in the aluminum matrix during cyclic crack tip propagation resulting in a concurrent increase in crack energy dissipation and a consequent increase in crack growth resistance. Plastic deformation during fatigue leads to crack nucleation either by separation of the silicon aluminum interface or by particle cracking or both.

Figure 9.27 shows experimental and modeling results from Kapoor et al. (2011) on fatigue of A206 alloy. This comprehensive paper on probabilistic modeling not

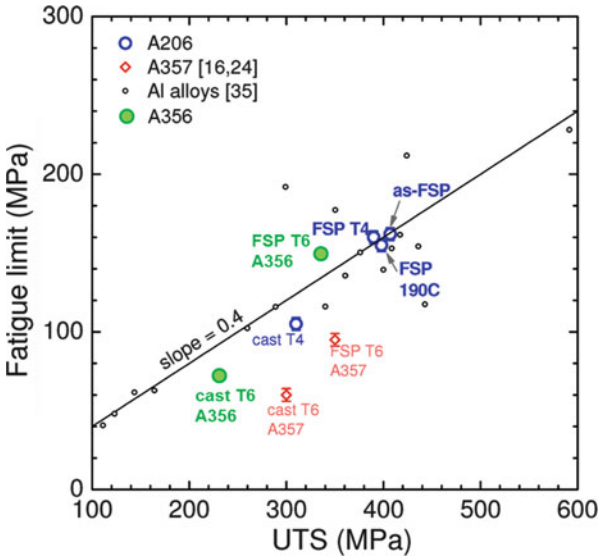

Fig. 9.28 Fatigue limit vs. UTS for A356, A357 and A206 aluminum alloys before and after FSP with different heat treatments. Compared are general data for other Al alloys (Figure taken from Kapoor et al. 2013, reprinted with permission from Elsevier, and modified to include A356 alloy data)

only focused on modeling prediction of the fatigue life of A206 specimens, but considered hypothetical specimens without any particles. Figure 9.27a shows the experimental and predicted data for A206 alloy. Clearly FSP leads to improvement in fatigue life. As discussed earlier, the fatigue life after FSP is controlled by largest flaw size, which in this case becomes broken down intermetallic particles. Then a hypothetical question arises; what is the maximum potential of FSP for fatigue life enhancement? In other words, if there were no flaws or large intermetallic particles, what would be the predicted life? The answer would then set the maximum limit of fatigue life enhancement that can be expected. Figure 9.27b has four curves. The cast + T4 data is the baseline and we are interested in the extent of improvement possible with FSP. The first two predicted lines are for two level of particle size distribution shown in inset. The assumption here is that FSP condition dictates the refinement of particles and these two examples are based on this. Again, a clear expectation is that the fatigue life would improve, which is consistent with all the experimental data. The last curve is for a material that has no particles. This condition represents the best case scenario where the FSP was so effective that it refined the entire particles to very small sizes where they are no longer fatigue crack nucleation sites, i.e. fatigue crack nucleation shifts to other types of sites.

The last point that we consider in this section is also taken from Kapoor et al. (2013). Figure 9.28 shows a plot of fatigue limit (stress for 10^7 cycles) with UTS for A356, A357 and A206. It is quite clear that FSP enhances the UTS and fatigue limit. This is the type of information that can be taken for design consideration.

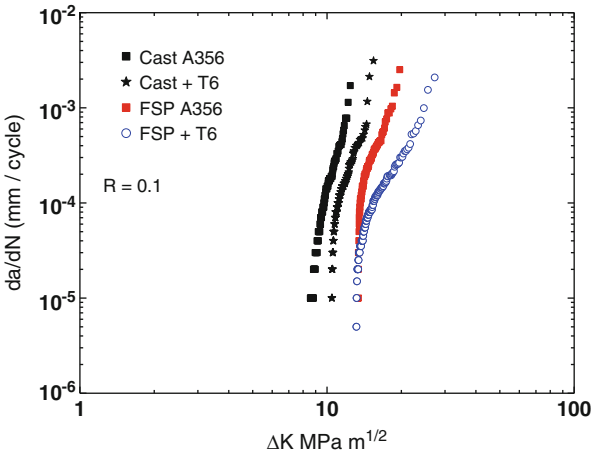

Fig. 9.29 Crack growth rates in A356 under various processing conditions at stress ratio R = 0.1 (Sharma and Mishra 2008, reprinted with permission from Elsevier)

Table 9.7 Comparison of "pseudo" fracture toughness of A356 under various processing conditions

	Cast	Cast + T6	FSP	FSP + T6
K_Q(MPa $\sqrt{m}$)	14.6 ± 2	15.8 ± 4	19.5 ± 1	24.4 ± 1

9.4.2.3 Fatigue Crack Growth and Fracture Toughness

There is not much data on fatigue crack growth. Figure 9.29 shows a comparison between the crack growth rates of cast A356 and friction stir processed region using compact tension specimen (Sharma and Mishra 2008). To achieve similar crack growth rates in FSP A356, compared to cast A356, a greater than 36 % increase in load was required. Also, the friction stir processed alloy follows region II in the da/dN vs. ΔK plot at higher ΔK values. The slower crack growth rates in FSP A356 are attributed to the finer microstructure developed during FSP. Results from tests conducted at higher stress ratios indicate that crack closure is the dominant mechanism in increasing crack growth resistance in FSP samples in the threshold region.

The upper limit of the crack driving force was assumed to be the "pseudo" fracture toughness of the materials. Because the CT specimens in that study did not meet plane strain fracture toughness requirements of ASTM E399, the measured fracture toughness values were referred to as "pseudo" fracture toughness. Pseudo fracture toughness was determined using the crack length and critical load at the onset of unstable fracture. The "pseudo" fracture toughness is only slightly influenced by the T6 heat treatment for the as-cast A356, while FSP samples show higher toughness than cast A356 samples, Table 9.7. The pseudo fracture toughness of FSP samples improved by over 30 % when compared to cast samples and in the T6 condition, FSP samples showed >50 % improvement in toughness.

9.5 Friction Stir Channeling (FSC)

During FSW, a defect referred to as a "wormhole" is generated if the processing parameters and tool shoulder contact are not proper. FSC is based on converting this defect formation process into a manufacturing technique for heat exchanger applications. Mishra (2005) has shown that a continuous hole in a single plate can be achieved by selecting the right processing conditions and reversing the material flow. Balasubramanian et al. (2009) published first paper on this concept and this section is taken from that paper. The main aspects of FSC are as follows:

(a) a profiled tool is rotated such that the material flow is upwards towards the tool shoulder,
(b) an initial clearance is provided between the shoulder and the workpiece, where the material from the base of the pin is deposited, and
(c) this distance between the tool shoulder and the workpiece can be adjusted to control the shape, size, and integrity of the channel.

The presence of the gap between the shoulder and the workpiece is a major difference between the FSC and the normal FSW or FSP practices where the back of the shoulder touches the workpiece to generate the forging action required to produce defect-free welding or processing. During channeling, an upward force is generated by rotating a right-hand threaded tool clockwise (or a left-hand threaded tool counter-clockwise). A channel is formed because of the separation of the plasticized material around the pin from the plasticized material at the base of the pin. This separated material is moved upwards by the rotation of the pin and the orientation of the threads, and it is deposited on the top of the nugget underneath the shoulder surface. The shape and size of the channel can be controlled by varying the following parameters: The clearance between the shoulder and the work material; the tool rotation speed; the tool traverse rate and the tool design.

The generation of a continuous channel by FSC has the potential to open a wide range of applications in heat exchanger industry. Heat exchangers are devices that are used to transfer thermal energy between two or more fluids, or between a solid surface and a fluid, at different temperatures and in thermal contact. Typical applications of heat exchangers involve heating or cooling of a fluid stream and evaporation or condensation of fluid streams, with an objective to reject or recover heat. Heat exchangers are usually classified on the basis of the transfer process, as either direct contact type or indirect contact type. The heat exchangers are also classified on the basis of the number of process fluids, or on the basis of the construction or flow arrangements or the heat transfer mechanisms. Another basis for classification of the heat exchangers is on the basis of surface compactness. The main objectives of compact heat exchangers are to maximize the efficiency of a heat exchanger and also to reduce the size of the heat exchanger for a given duty. Compact heat exchangers are generally used in industry, especially in gas-to-gas or liquid-to-gas heat exchangers. For example, vehicular heat exchangers, condensers and evaporators in air-condition and refrigeration industry, aircraft oil-coolers, automotive radiators, and intercoolers or compressors.

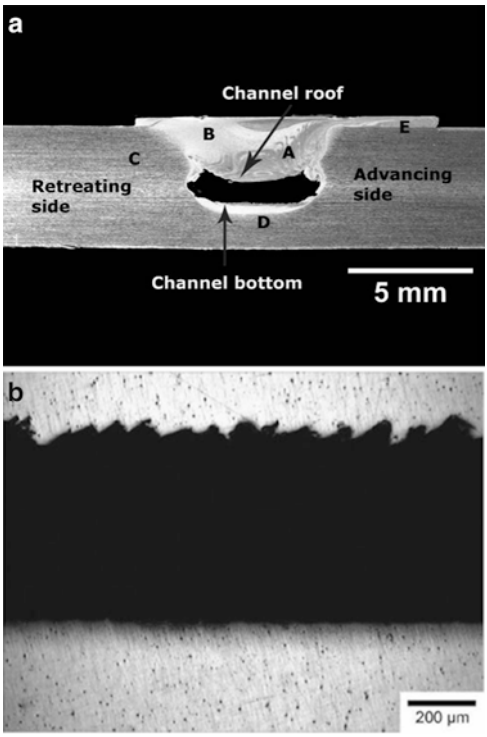

Fig. 9.30 (**a**) Cross-sectional image of a channel showing the different process regions: (A + B) channel nugget, (C) parent material, (D) channel, and (E) material from the channel nugget deposited on the surface. (**b**) Longitudinal cross section of the channel showing the roughness on the roof of the channels (800 rpm, 1.27 mm/s) (Taken from Balasubramanian et al. 2009, reprinted with permission from Elsevier)

Figure 9.30 shows the cross section of the channel nugget, and depicts clearly the material flow pattern during the process, after the tool has passed the region. The direction of tool rotation is counter clockwise and the traverse direction is into the plane of the paper. To understand the channel formation requires distinguishing among the different regions of the channel cross section. Regions A and B are collectively referred to as the stir zone. Region C is the unprocessed parent material, and region D is the channel. Region E represents the material deposited from the channel nugget region above the original surface of the material, underneath the shoulder. To allow a channel to form, material must be removed from the stir zone. This is accomplished by having a space between the tool shoulder and top surface of the workpiece, and allows the pin features to move the material in this gap. Because of the orientation of the threads on the pin and the direction of tool rotation, the plasticized region at the bottom of the channel is pushed upward on the advancing side (the side where the tool surface velocity vector is opposite to the tool traverse direction). The upward force produced by the threads causes the plasticized material to be pushed upward and deposited by the shoulder on the surface (region E). Region A represents the part of the nugget processed by the pin. The pattern seen in region A depicts the flow path of the material moving from the pin base to the shoulder-workpiece clearance.

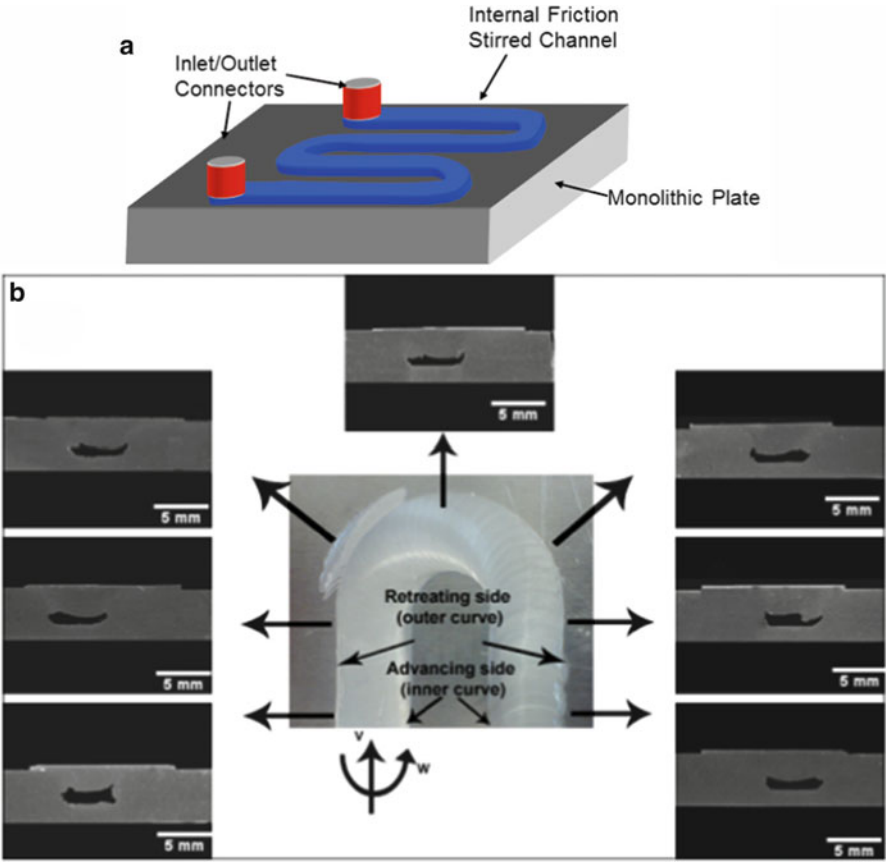

Fig. 9.31 (**a**) Conceptual depiction of a heat exchanger fabricated by robotic machine. (**b**) Also included is a curved channel example from Balasubramanian et al. (2009), reprinted with permission from Elsevier

The deposition of the material underneath the shoulder results in a downward resultant force on the channel roof behind the pin (trailing side of the tool). Also, due to the shoulder rotation, the material in the upper region of the workpiece is pushed inward and deposited in region B, mainly on the retreating side. An additional layer surrounds the nugget, referred to as a thermo-mechanically affected zone (TMAZ), where the amount of grain refinement is insignificant. TMAZ is unclear in Fig. 9.30. The surface roughness at the upper surface of the channel is uniformly spaced, and the periodicity of the roughness at the top surface matches the amount of material that is being displaced with each rotation, i.e., the process pitch. In the case of Fig. 9.30b, the pitch of the run is 0.095 mm/rot, and the actual spacing is 0.091 mm.

Figure 9.31 shows a conceptual drawing of a heat exchanger from a single plate. Also included is a figure from Balasubramanian et al. (2009), which shows the channel along a curved friction stir channeling run with a robotic machine. This is a technique that shows friction stir processing as a manufacturing technique.

9.6 Ultrafine Grained Materials via Friction Stir Processing

Ultrafine grained materials (UFG) are of interest because it provides a balance between strength, ductility and other properties. It also provides unique opportunities to investigate dislocation based plasticity mechanisms. Some reference to ultrafine grained microstructure (referred as average grain size below 1 μm) has come in earlier chapter and in this chapter in the context of powder metallurgy alloys and superplasticity. In this section, we capture a few examples of microstructure and room temperature behavior.

Figure 9.32 shows an ultrafine grained Al-4 Mg- 1 Zr alloy with truly random grain misorientation distribution. Such microstructure is unheard of from conventional thermo-mechanical processing (TMP) techniques. The average grain size of this UFG alloy is ~700 nm with >97 % HAGB in FSP Al-Mg-Zr specimen. For comparison, conventional TMP for superplastic sheet leads to ~60 % HAGB and equal channel angular pressing (ECAP) leads to around 80 % HAGB in eight passes. ECAP is routinely used to obtain UFG microstructure and severe plastic deformation community relies heavily on this technique. FSP has proven to a very effective severe plastic deformation technique because of unique combination of high strain, high strain rate and high processing temperature.

A scientifically important result was published by Kumar et al. (2011) on critical grain size for dislocation plasticity and intragranular dislocation storage. Figure 9.33 shows two ultrafine grained conditions designated as UFG-1 and UFG-2. The average grain size only changed from 0.63 to 0.39 μm, however the stress-strain curves are quite different in terms of uniform elongation and strain hardening (Fig. 9.34). Kumar et al. (2011) explained this on the basis of dislocation-dislocation interaction within the grain and possibility of dislocation storage.

Similar behavior was also reported by Panigrahi et al. (2012) as shown in Fig. 9.35. The stress-strain curves in four conditions are very illustrative of change

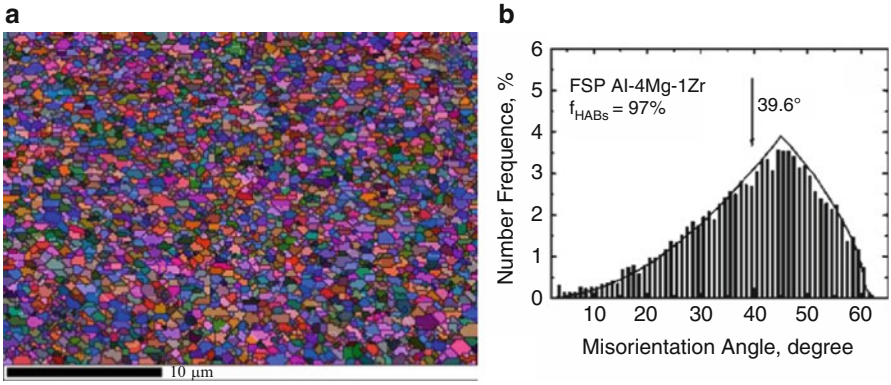

Fig. 9.32 (**a**) An orientation imaging map of Al-4 Mg-1 Zr alloy showing ultrafine grained microstructure and (**b**) a truly random misorientation distribution (Ma et al. 2010, reprinted with permission from Elsevier)

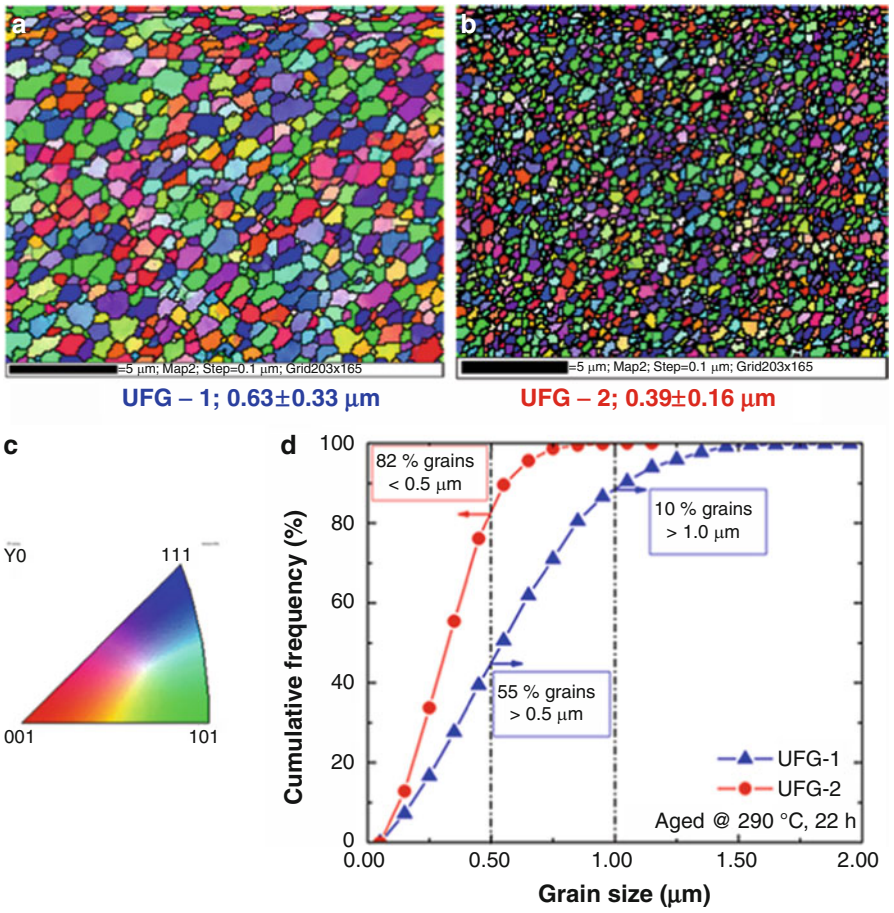

Fig. 9.33 (**a**, **b**) Micrographs of Al-Mg-Sc alloy in two ultrafine grained conditions. (**c**) Inverse pole figures with colors used for figures in (**a**) and (**b**). (**d**) Cumulative frequency distribution of grain size for both conditions (Kumar et al. 2011, reprinted with permission from Elsevier)

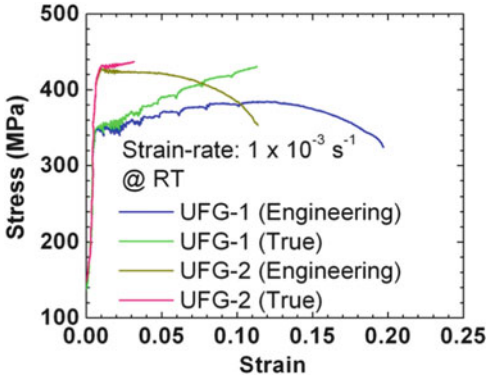

Fig. 9.34 The stress-strain behavior for the microstructures shown in Fig. 9.33. Note the difference in the work hardening and uniform elongation. The true stress-true strain curve is only plotted till uniform elongation (Kumar et al. 2011, reprinted with permission from Elsevier)

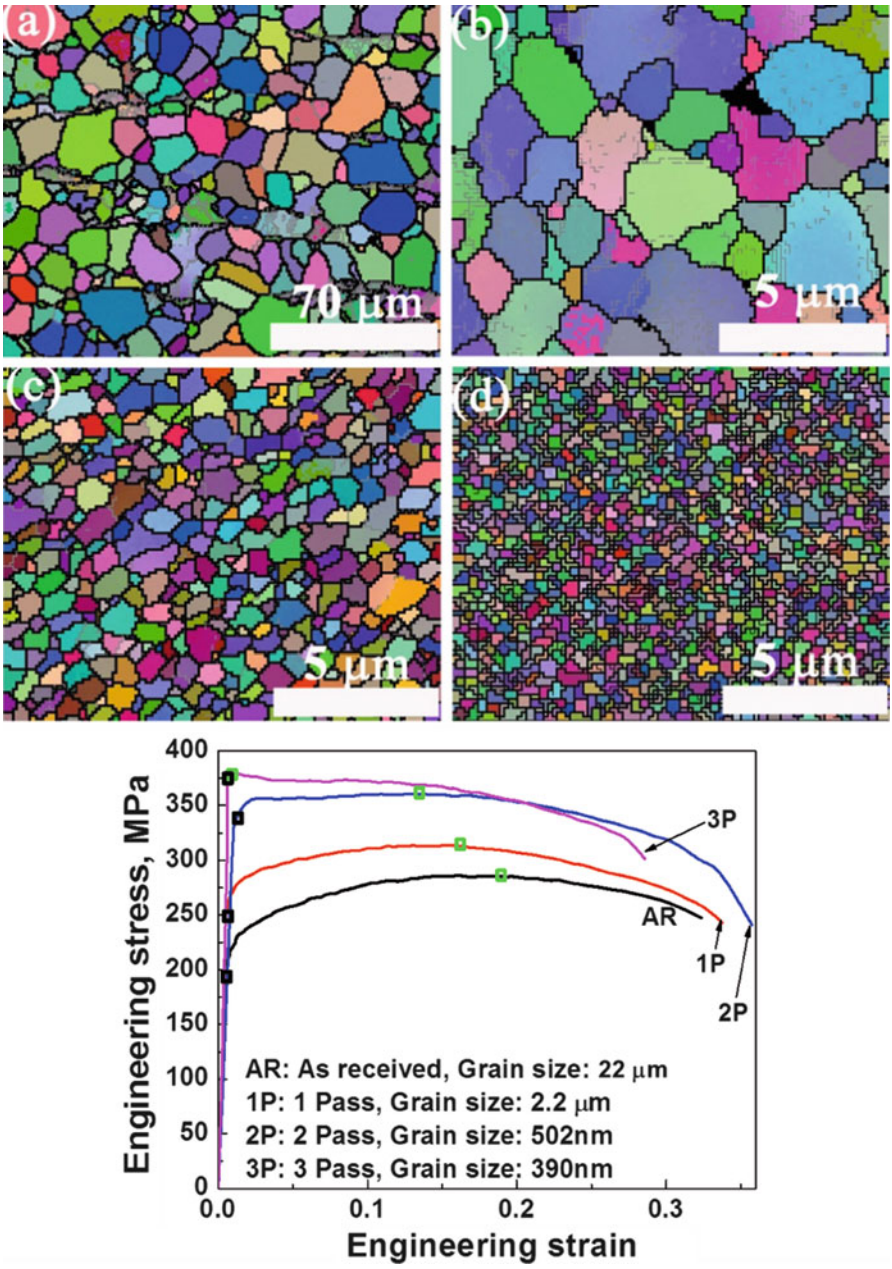

Fig. 9.35 (**a**)–(**d**) Microstructure of a WE43 magnesium alloy in four conditions and (**e**) associated stress-strain curves. Note the lack of work hardening in the UFG material with 390 nm average grain size (Panigrahi et al. 2012, reprinted with permission from Elsevier)

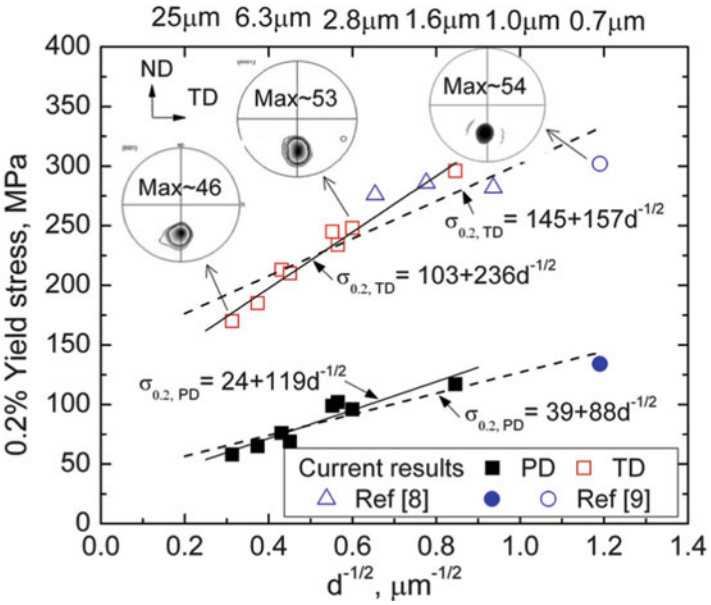

Fig. 9.36 Variation of yield strength with grain size in FSP AZ31 magnesium alloy. These specimens exhibited significantly strong texture as shown in the *inset* pole figures (Yuan et al. 2011, reprinted with permission from Elsevier)

in deformation mechanisms. It can be noted that the finest UFG material with 390 nm average grain size, the yield stress is quite high and there is no work hardening. Still the specimen exhibited significant overall ductility. This is a common trend now among FSP materials. Panigrahi et al. (2012) also correlated this transition to deformation by twinning in Mg alloys. They observed that UFG alloys showed no twinning. An interesting aspect in magnesium alloys is the extent of texture during FSP. The OIM micrographs in Fig. 9.35 show random orientation of grains. On the other hand, a study by Yuan et al. (2011) on single phase AZ31 magnesium alloy showed that texture can be very significant as shown in the inset of Fig. 9.36. They took advantage of this to investigate the role of grain size and texture on the Hall-Petch relationship (grain boundary strengthening). The approach used to obtain ultrafine grain size without any external cooling involved using overlapping passes with reduced heat during successive passes by lowering the tool rotation rate. This shows that the processing parameters can be controlled to obtain microstructure with different level of texture and grain refinement.

References

M.F. Ashby, Designing hybrid materials. Acta Mater. **51**, 5801 (2003)
W.A. Backofen, I.R. Turner, D.H. Avery, Superplasticity in an Al-Zn alloy. Trans. ASM **57**, 980–989 (1964)
N. Balasubramanian, R.S. Mishra, K. Krishnamurthy, Friction stir channeling: characterization of the channels. J. Mater. Process. Technol. **209**(8), 3696–3704 (2009)
P.B. Berbon, W.H. Bingel, R.S. Mishra, C.C. Bampton, M.W. Mahoney, Friction stir processing: a tool to homogenize nanocomposite aluminum alloys. Scr. Mater. **44**, 61 (2001)
I. Charit, R.S. Mishra, Low temperature superplasticity in a friction-stir-processed ultrafine grained Al-Zn-Mg-Sc alloy. Acta Mater. **53**(15), 4211–4223 (2005)
J. Datsko, C.T. Yang, Correlation of bendability of materials with their tensile properties. Trans. ASME B **82**(4), 309–313 (1960)
M. Dixit, J.W. Newkirk, R.S. Mishra, Properties of friction stir-processed Al 1100-NiTi composite. Scr. Mater. **56**, 541–544 (2007)
M. Drouzy, S. Jacob, M. Richard, Interpretation of tensile results by means of a quality index. AFS Int. Cast Metal J. **5**, 43–50 (1980)
J.D. Eshelby, Proc. Roy. Soc. Lond. **A241**, 376 (1957)
G.J. Grant, D. Herling, W. Arbegast, C. Allen, C. Degen, *2006 International Conference on Superplasticity in Advanced Materials*, Chengdu, China, 23 June 2006
Z. Hashin, S. Strikman, J. Appl. Phys. **33**, 3125 (1962)
S.M. Howard, B.K. Jasthi, W.J. Arbegast, G.J. Grant, D.R. Herling, Friction surface reaction processing in aluminum substrates. Friction stir welding and processing III as held at the 2005 TMS annual meeting, San Francisco, CA, 2005, pp. 139–146
L.B. Johannes, L.L. Yowell, E. Sosa, S. Arepalli, R.S. Mishra, Survivability of single-walled carbon nanotubes during friction stir processing. Nanotechnology **17**, 3081–3084 (2006)
R. Kapoor, V.S.H. Rao, R.S. Mishra, J.A. Baumann, G. Grant, Probabilistic fatigue life prediction model for alloys with defects: applied to A206. Acta Mater. **59**(9), 3447–3462 (2011)
R. Kapoor, K. Kandasamy, R.S. Mishra, J.A. Baumann, G. Grant, Effect of friction stir processing on the tensile and fatigue behavior of a cast A206 alloy. Mater. Sci. Eng. A **561**, 159–166 (2013)
N. Kumar, R.S. Mishra, C.S. Huskamp, K.K. Sankaran, Critical grain size for change in deformation behavior in ultrafine grained Al-Mg-Sc alloy. Scr. Mater. **64**(6), 576–579 (2011)
C.J. Lee, J.C. Huang, P.J. Hsieh, Mg based nano-composites fabricated by friction stir processing. Scr. Mater. **54**, 1415–1420 (2006a)
C.J. Lee, J.C. Huang, P.L. Hsieh, Compos. Mater. **313**, 69 (2006b)
Z.Y. Ma, R.S. Mishra, Friction stir surface composite fabrication. Surface engineering: in materials science II, TMS, Warrendale, PA, 2003, p. 243
Z.Y. Ma, R.S. Mishra, M.W. Mahoney, Superplasticity in cast A356 induced via friction stir processing. Scr. Mater. **50**(7), 931–935 (2004)
Z.Y. Ma, F.C. Liu, R.S. Mishra, Superplastic deformation mechanism of an ultrafine-grained aluminum alloy produced by friction stir processing. Acta Mater. **58**(14), 4693–4704 (2010)
M. Mahoney, R.S. Mishra, T. Nelson, J. Flintoff, R. Islamgaliev, Y. Hovansky, High strain rate, thick section superplasticity created via friction stir processing. Friction stir welding and processing, Indianapolis, IN, 4–8 Nov 2001, pp. 183–194
R.S. Mishra, M.W. Mahoney, S.X. McFadden, N.A. Mara, A.K. Mukherjee, High strain rate superplasticity in a friction stir processed 7075 al alloy. Scr. Mater. **42**, 163 (1999)
R.S. Mishra, M.W. Mahoney, in *Friction Stir Processing: A New Grain Refinement Technique To Achieve High Strain Rate Superplasticity in Commercial Alloys*. Superplasticity in Advanced Materials, ICSAM-2000 Materials Science Forum, 357–3 (2001), p. 507
R.S. Mishra, M.W. Mahoney, U.S. Patent (6,712,916) on "Metal superplasticity enhancement and forming process," 30 Mar 2004

R.S. Mishra, M.W. Mahoney, *Friction Stir Processing, in Friction Stir Welding and Processing,* ed. by R.S. Mishra, M.W. Mahoney (ASM International, Materials Park, 2007), pp. 309–350. ISBN-13: 978-0-87170-840-3

R.S. Mishra, Friction stir processing for superplasticity. Adv. Mater. Process. **162**(2), 45–47 (2004)

R.S. Mishra, Integral channels in metal components, U.S. Patent 6,923,362, 2005

R.S. Mishra, Z.Y. Ma, I. Charit, Friction stir processing: a novel technique for fabrication of surface composite. Mater. Sci. Eng. A **A341**, 307 (2003)

R.S. Mishra, M.W. Mahoney, Metal superplasticity enhancement and forming process, U.S. Patent 6,712,916, 30 March 2004

Y. Morisada, H. Fujii, T. Nagaoka, M. Fukusumi, Structural materials properties microstructure and processing. Mater. Sci. Eng. **419**, 344 (2006)

Y. Murakami, M. Endo, Effects of defects, inclusions and inhomogeneities on fatigue strength. Int. J. Fatig. **16**, 163–182 (1994)

J.W. Newkirk, R. Mishra, J. Thomas, J.A. Hawk, Friction stir processing to create surface composites. Advances in powder metallurgy & particulate materials, MPIF, Princeton, NJ, 2003, pp. 6.60–6.70

T.G. Nieh, J. Wadsworth, O.D. Sherby, *Superplasticity in Metals and Ceramics* (Cambridge University Press, Cambridge, UK, 1997)

S.K. Panigrahi, K. Kumar, N. Kumar, W. Yuan, R.S. Mishra, R. DeLorme, B. Davis, R.A. Howell, K. Cho, Transition of deformation behavior in an ultrafine grained magnesium alloy. Mater. Sci. Eng. A **549**, 123–127 (2012)

U. Ramadorai, J.W. Newkirk, R.S. Mishra, J.A. Hawk, *Surface Modification of Aluminum Alloys to Create in Situ Surface Composites*. 4th ASM International Surface Engineering Congress and 19th International Conference on Surface Modification Technologies, August 2005

S.R. Sharma, R.S. Mishra, Fatigue crack growth behavior of friction stir processed aluminum alloy. Scr. Mater. **59**(2008), 395–398 (2008)

S.R. Sharma, Z.Y. Ma, R.S. Mishra, Effect of friction stir processing on fatigue behavior of A356 alloy. Scr. Mater. **51**(3), 237–241 (2004)

C.B. Smith, R.S. Mishra, *Friction Stir Processing for Enhanced Low Temperature Formability: A Volume in the Friction Stir Welding and Processing Book Series* [Paperback] (2014). ISBN-10: 012420113X

J.E. Spowart, Z.-Y. Ma, R.S. Mishra, The effect of friction stir processing (FSP) on the spatial heterogeneity of discontinuously-reinforced aluminum (DRA) microstructures. Friction stir welding and processing II, 2003 TMS annual meeting, San Diego, CA, 2–6 Mar 2003, pp. 243–252

S. Tandon and R. S. Mishra, unpublished research

Y. Wang and R.S. Mishra, Finite element simulation of selective superplastic forming of friction stir processed 7075 Al alloy, Materials Science and Engineering A, **463**, 245–248. (2007)

W. Yuan, S.K. Panigrahi, J.-Q. Su, R.S. Mishra, Influence of grain size and texture on Hall-Petch relationship for a magnesium alloy. Scr. Mater. **65**(11), 994–997 (2011)

J. Zheng, R.S. Mishra, P.B. Berbon, M.W. Mahoney, Microstructure and mechanical behavior of friction stir processed Al-Ti-Cu alloy. Friction stir welding and processing, Indianapolis, IN, 4–8 Nov 2001, pp. 235–242